

Accreting Millisecond X-Ray Pulsars

A. Patruno, A. L. Watts

Abstract Accreting Millisecond X-Ray Pulsars (AMXPs) are astrophysical laboratories without parallel in the study of extreme physics. In this chapter we review the past fifteen years of discoveries in the field. We summarize the observations of the fifteen known AMXPs, with a particular emphasis on the multi-wavelength observations that have been carried out since the discovery of the first AMXP in 1998. We review accretion torque theory, the pulse formation process, and how AMXP observations have changed our view on the interaction of plasma and magnetic fields in strong gravity. We also explain how the AMXPs have deepened our understanding of the thermonuclear burst process, in particular the phenomenon of burst oscillations. We conclude with a discussion of the open problems that remain to be addressed in the future.

1 Introduction

Neutron stars (NSs), amongst the most extreme astrophysical objects in the Universe, allow us to study physics in regimes that cannot be accessed by terrestrial laboratories. They play a key role in the study of fundamental problems including the equation of state (EoS) of ultra-dense matter, the production of gravitational waves, dense matter superfluidity and superconductivity, and the generation and evolution of ultra-strong magnetic fields. Since the discovery of NSs as radio pulsars in 1967 [1], many different classes have been discovered including more than ~ 130 NSs in low mass X-ray binaries (LMXBs). In LMXBs the NS accretes mat-

A. Patruno
Leiden Observatory, Huygens Laboratory, Leiden University, Neils Bohrweg 2, 2333 CA, Leiden,
The Netherlands; e-mail: patruno@strw.leidenuniv.nl
A.L. Watts
Astronomical Institute “Anton Pannekoek”, University of Amsterdam, Science Park 904, 1098 XH,
Amsterdam, The Netherlands; e-mail: a.l.watts@uva.nl

ter from a non-collapsed stellar companion (with mass $M \lesssim 1 M_{\odot}$) via an accretion disk. This chapter focuses on a subgroup of the LMXBs, the accreting millisecond X-ray pulsars (AMXPs). In the AMXPs, the gas stripped from the companion is channeled out of the accretion disk and onto the magnetic poles of the rotating neutron star, giving rise to X-ray pulsations at the spin frequency. We will explore the details of this process, why it is so rare (the AMXPs are a small class), the physics of the disk-magnetosphere interaction, and how AMXPs can be used to probe extreme physics.

Immediately after the discovery of the first millisecond radio pulsar in 1982 [2], LMXBs were identified as possible incubators for millisecond pulsars. It was suggested that LMXBs might be responsible for the conversion of slow NSs with high magnetic field ($B \sim 10^{12}$ G), into a rapidly spinning objects with a relatively weak magnetic field ($B \sim 10^8$ G). Two independent papers published in 1982 [3, 4] proposed transfer of angular momentum through accretion as the mechanism responsible for the spin-up of pulsars. This is known as the *recycling scenario* (see [5] for an excellent review). This name originates from the fact that radio pulsars switch off their pulsed radio emission after entering the so-called “pulsar graveyard”. If this happens while the NS is in a binary with a non-collapsed low or intermediate mass stellar companion, binary evolution of the system [6, 7] can bring the companion into Roche lobe contact and trigger a prolonged epoch of mass transfer from the companion (donor) towards the NS (accretor). The mass is transferred with large specific angular momentum and the NS is spun-up by the resulting accretion torques. Once the mass transfer episode terminates, the NS might eventually switch on again as a “recycled” millisecond radio pulsar.

The first AMXP (SAX J1808.4–3658), found in 1998 with the *Rossi X-ray Timing Explorer (RXTE)* [8] provided a beautiful confirmation of the recycling scenario. Fourteen more AMXPs have since been found, with spin frequencies from 182 to 599 Hz. Another important milestone came with the discovery (in 2007) of a binary radio millisecond pulsar (PSR J1023+0038) for which archival optical observations, taken ~ 7 years before the radio pulsar discovery, showed evidence for an accretion disk¹ [11]. This is the first NS observed to have switched on as a radio pulsar after being an X-ray binary. A final confirmation that indeed AMXPs and radio pulsars are related has recently come with the discovery of the system IGR J18245–2452 which has shown both an AMXP and a radio millisecond pulsar phase (see [12] and Section 3.15 for a detailed discussion).

The *RXTE* observatory has played an extraordinary role by discovering many systems of this kind and by collecting extensive data records of each outburst detected during its fifteen year lifetime. The excellent timing capabilities of *RXTE* have brought new means to study NSs with coherent X-ray timing, and helped to constrain the long term properties of many AMXPs over a baseline of more than a decade. Observation of the orbital Doppler shift of the AMXP pulse frequency contains information on the orbital parameters of the binary and their evolution in time. Binary evolution has benefited from the study of AMXPs [13, 14, 15] which

¹ a new transition from a radio pulsar to a LMXB has happened and is currently ongoing at the moment of writing this review [9, 10]

are now known to include ultra-compact systems (orbital period $P_b \lesssim 80$ min) with white dwarf companions, compact systems ($P_b \simeq 1.5 - 3$ hr) with brown dwarf donors and wider systems ($P_b \simeq 3.5 - 20$ hr) with main sequence stars. Other X-ray and gamma ray space missions like *XMM-Newton*, *INTEGRAL*, *Chandra*, *Swift* and *HETE* have also played an important role in discovering and understanding the spectral and timing properties of these objects. Multiwavelength observations covering radio, infrared, optical and UV wavelengths have also illuminated different aspects of these fascinating systems. Several optical and infrared counterparts have been identified with ground based observations and in some cases have led to the discovery of the spectral type of the donor, while radio and infrared observations have revealed the possible presence of jets.

This chapter is structured as follows:

- Section 2.** An overview of the AMXP family.
- Section 3.** Observations of individual AMXPs
- Section 4.** Coherent timing analysis and accretion torques.
- Section 5.** X-ray pulse properties, their formation and use.
- Section 6.** Long-term evolution of spins and orbital parameters.
- Section 7.** Thermonuclear bursts and burst oscillations.
- Section 8.** Aperiodic phenomena including kilohertz QPOs.
- Section 9.** Future developments and open questions.

2 The Accreting Millisecond X-ray Pulsar Family

An AMXP is an accretion powered X-ray pulsar spinning at frequencies $\nu \geq 100$ Hz bound in a binary system with a donor companion of mass $M \lesssim 1 M_\odot$ and with weak surface magnetic fields ($B \sim 10^{8-9}$ G). All known AMXPs have donor stars that transfer mass via Roche lobe overflow (RLOF). This definition excludes binary millisecond pulsars, which are detached systems with a pulsar powered by its rotational energy, X-ray pulsars in high mass X-ray binaries, symbiotic X-ray binaries and the slow X-ray pulsars in LMXBs with $\nu < 100$ Hz. Several LMXBs show millisecond oscillations during thermonuclear bursts that ignite on their surface. These nuclear powered X-ray pulsars (NXPs), or burst oscillation sources, are not AMXPs, since they are powered by nuclear burning rather than channeled accretion (although note that some AMXPs also show burst oscillations).

Table 1 reports the main characteristics of the 23 known pulsating NSs in LMXBs: 15 AMXPs, 3 slow accreting X-ray pulsars in LMXBs, 1 slow accreting X-ray pulsar in an intermediate mass X-ray binary (IMXB), 3 symbiotic X-ray binaries accreting wind from a K/M giant companion (compatible with being of low mass type) and 1 mildly recycled accreting pulsar recently discovered in the globular cluster Terzan 5. This latter source is an 11 Hz X-ray pulsar with a magnetic field of $10^9 - 10^{10}$ G and is of particular interest because it might be the only known accreting pulsar in the process of becoming an AMXP on a short timescale [16].

The other four slow pulsars are very different systems, in the sense that they have most likely followed a completely different evolutionary history, have strong magnetic fields ($B \sim 10^{12}$ G) and may never reach millisecond periods. Symbiotic X-ray binaries are also different from the AMXPs since they are wide binaries ($P_b \gtrsim 50$ days) and their NSs have extremely long spin periods caused by a prolonged phase of spin-down during a wind accretion process.

All of the AMXPs are transient systems, with accretion disks that run through cycles of outburst and quiescence. X-ray pulsations have never been observed in quiescence, although the upper limits are unconstraining due to the poor photon flux. The shortest outburst recurrence time is one month for the globular cluster source NGC 6440 X-2, with an outburst duration of less than 4-5 days, whereas the longest outburst, from HETE J1900.1-2455, has so far lasted for almost 7 years. The small group of AMXPs therefore form a rather heterogeneous class of objects. There are, however, some common features shared by all AMXPs:

- Outburst luminosities are usually faint, suggesting low time averaged mass accretion rates (Section 3).
- Spin frequencies appear to be uniformly distributed with an abrupt cutoff at about ~ 700 Hz (Section 6).
- Ultra-compact binaries are rather common, comprising about 40% of the total AMXP population.
- Very small donors are preferred, with masses almost always below $0.2 M_{\odot}$.
- The orbital periods are always relatively short, with $P_b < 1$ day. Therefore the known AMXPs are probably **not** the progenitors of wide orbit binary millisecond radio pulsars.

2.1 Intermittency

Until 2007 it was believed that AMXPs showed X-ray pulsations throughout outbursts. The seventh AMXP (HETE J1900.1-2455), however, showed an unexpected new behaviour [63]. For the first ≈ 20 days of its outburst (which started in 2005) it showed typical AMXP pulsations. The pulsations then became intermittent, appearing and disappearing on different timescales for the next ≈ 2.5 years. Pulsation disappeared and never reappeared again after MJD 54,499 [64], with the most stringent upper limits of 0.05% rms on the fractional pulse amplitude (i.e., a sinusoidal fractional amplitude of 0.07%, see Eq. 15).

This discovery was exciting, since it may help to bridge the gap between non-pulsating LMXBs and AMXPs. It also became immediately clear that other LMXBs might show sporadic episodes of pulsations during their outbursts. This has now been found to be the case for two other sources: Aql X-1 and SAX J1748.9-2021.

Table 1 Accreting X-ray Pulsars in Low Mass X-ray Binaries

Source	ν_s (Hz)	P_b (hr)	f_x (M_\odot)	$M_{c,min}$ (M_\odot)	Companion Type	Ref.
Accreting Millisecond Pulsars						
SAX J1808.4–3658	401	2.01	3.8×10^{-5}	0.043	BD	[17, 18, 19, 20, 21]
XTE J1751–305	435	0.71	1.3×10^{-6}	0.014	He WD	[22, 23]
XTE J0929–314	185	0.73	2.9×10^{-7}	0.0083	C/O WD	[24, 25, 123]
XTE J807–294	190	0.67	1.5×10^{-7}	0.0066	C/O WD	[26, 27, 28, 29, 30]
XTE J1814–338	314	4.27	2.0×10^{-3}	0.17	MS	[31, 32]
IGR J00291+5934	599	2.46	2.8×10^{-5}	0.039	BD	[33, 34, 35, 36, 37, 38]
HETE J1900.1–2455	377	1.39	2.0×10^{-6}	0.016	BD	[39]
Swift J1756.9–2508	182	0.91	1.6×10^{-7}	0.007	He WD	[40, 41]
Aql X–1	550	18.95	N/A	0.6 ^a	MS	[42, 43]
SAX J1748.9–2021	442	8.77	4.8×10^{-4}	0.1	MS/SubG ?	[44, 45]
NGC6440 X–2	206	0.95	1.6×10^{-7}	0.0067	He WD	[46]
IGR J17511–3057	245	3.47	1.1×10^{-3}	0.13	MS	[47, 48]
Swift J1749.4–2807	518	8.82	5.5×10^{-2}	0.59	MS	[49]
IGR J17498–2921	401	3.84	2.0×10^{-3}	0.17	MS	[50]
IGR J18245–2452	254	11.03	2.3×10^{-3}	0.17	MS	[12]
Mildly Recycled X-ray Pulsar						
IGR J17480-2466	11	21.27	2.1×10^{-2}	0.4	SubG	[51, 52, 53]
Slow Pulsars in LMXBs & IMXBs						
2A 1822-371	1.7	5.57	2×10^{-2}	0.33	?	[54]
4U 1626-67	0.13	0.69	1.3×10^{-6}	0.06	WD or He star	[55, 56, 57]
GRO 1744-28	2.14	282.24	1.3×10^{-4}	< 0.3	Giant	[55, 58, 59]
Her X-1	0.81	40.80	0.85	$\sim 2^a$	MS	[55, 57]
Symbiotic X-ray Binaries						
GX 1+4	6.3×10^{-3}	1161 days			M5 Giant	[58, 60, 61]
4U 1954+31	5.5×10^{-5}				M4 Giant	[62, 61]
IGR J16358–4724 ^b	1.7×10^{-4}				K/M Giant	[62, 61]

ν_s is the spin frequency, P_b the orbital period, f_x is the X-ray mass function, $M_{c,min}$ is the minimum companion mass for an assumed NS mass of $1.4 M_\odot$. The companion types are: WD = White Dwarf, BD= Brown Dwarf, MS = Main Sequence, SubG = Sub-Giant, He Core = Helium Star.

^a The donor mass is inferred from photometric data and does represent the most likely mass.

^b Binary with parameters that are still compatible with an intermediate/high mass donor.

Aql X–1 is perhaps the most striking case recorded so far: coherent pulsations were discovered in 1998 *RXTE* archival data and appeared in only one 120s data segment out of a total exposure time of 1.5 Ms from more than 10 years of observations. The extremely short pulse episode has raised discussions about whether it really originated from magnetic channeled accretion, and whether Aql X-1 can truly be considered an AMXP. However, the high coherence of the signal leaves little doubt about the presence of pulsations, and the accretion-powered origin appears the most promising explanation [42]. The case of SAX J1748.9–2021 is slightly different: pulsations were detected sporadically in several data segments and in three (2001, 2005 and 2009-2010 [45, 44, 65]) out of four outbursts observed (the first being in 1998). It is unclear why these three systems show pulsations intermittently. In HETE J1900.1–2455, an increase in pulse fractional amplitude was reported approximately in coincidence with the occurrence of Type I X-ray bursts [63], followed by a steady decrease. On other occasions the pulsations appeared a few hours before or after a burst, indicating that pulsations might be linked somehow with some yet to be iden-

tified property of the NS envelope. In SAX J1748.9–2021 the pulsed amplitudes showed some abrupt changes in amplitude and/or phase in coincidence with about 30% of the observed Type I X-ray bursts [45, 44]. The pulsations, however, displayed a more diverse behaviour than in HETE J1900.1–2455, without the typical steady decrease of fractional amplitudes. A period of global surface activity during which both Type I bursts and pulsations are produced might be at the origin of this link [44]. The single pulsating episode of Aql X-1 had instead no clear connection with Type I bursts, even though Aql X-1 is a bursting LMXB.

The spin frequency derivative of HETE J1900.1–2455 was measured over a baseline of 2.5 years, an unprecedented long baseline for an AMXP (whose outbursts last usually less than 100 days). This has indirectly provided hints on the physical origin of such a period of global surface activity in intermittent sources. The spin frequency derivative exhibited an exponential decay in time that was interpreted as evidence of the screening of the NS magnetic field [64]. It was proposed that intermittency originates because the magnetic field strength drops by almost three orders of magnitude on a timescale of few hundred days so that the disk cannot be truncated and only a (very) shallow layer of gas can be channeled to form (weak) pulsations (see also Section 6.3 for a discussion of the model).

One feature that intermittent pulsars share is that the long term average mass accretion rate $\langle \dot{M} \rangle$ is higher than for the persistent AMXPs and smaller than for the bright non-pulsating systems (like Sco X-1 and the other Z sources). Calculating the precise value of $\langle \dot{M} \rangle$ is rather difficult, since it depends on poorly constrained parameters in most LMXBs, like the distance d , the X-ray to bolometric flux conversion and the recurrence time of the outburst. However, even considering these caveats, it seems clear that at least the brightest systems have never showed pulsations. Whether it is the high mass accretion rate that determines the lack of pulsations or some other properties shared by the brightest systems is still unclear. See Section 6 for an extended discussion on the mechanism that might prevent the formation of pulsations in LMXBs.

3 Observations of the AMXPs

In this section we discuss the main characteristics of each AMXP, including number of outbursts observed, luminosity, distance, orbital parameters and (at the end of each subsection) radio/IR/optical counterparts. We devote Section 4 and 6 to the discussion of the results on the pulsar rotational parameters and their secular evolution, respectively. We briefly mention results relating to X-ray bursts, burst oscillations and aperiodic variability but refer to Section 7 and 8 for a general discussion of these topics. The astrometric position of each AMXP is given in Table 2.

Table 2 Astrometric Position of AMXPs

Source	Right Ascension [HH:MM:SS] (J2000)	Declination [DD:MM:SS] (J2000)	Error (90% c.l.)	Observatory	Reference
SAX J1808.4–3658	18:08:27.62	-36:58:43.3	0".15	6.5 m Baade (Magellan I)	[18]
XTE J1751–305	17:51:13.49(5)	-30:37:23.4(6)		Chandra	[22]
XTE J1807–294	18:06:59.80	-29:24:30	0".6	Chandra	[26]
IGR J00291+5934	00:29:03.05(1)	+59:34:18.93(5)		Multiple Optical Obs.	[66]
XTE J1814–338	18:13:39.04	-33:46:22.3	0".2	Magellan	[67]
XTE J0929–314	09:29:20.19	-31:23:03.2	0".1	Mt. Canopus	[68]
Swift J1756.9–2508	17:56:57.35	-25:06:27.8	3".5	Swift/XRT	[40]
Aql X–1	19:11:16.0245341	+00:35:05.879384	0".0005	e-EVN	[69]
SAX J1748.9–2021	17:48:52.163	-20:21:32.40	0".6	Chandra	[70]
NGC6440 X-2	17:48:52.76(2)	-20:21:24.0(1)		Chandra	[71]
Swift J1749.4–2807	17:49:31.83	-28:08:04.7	1".6	Swift/XRT	[72]
IGR J17511–3057	17:51:08.66(1)	-30:57:41.0(1)	0".6	Chandra	[73]
IGR J17498–2921	17:49:55.38	-29:19:19.7	0".6	Chandra	[74]
HETE J1900.1–2455	19:00:08.65	-24:55:13.7	0".2	Palomar	[75]
IGR J18245–2452	18:24:32.51	-24:52:07.9	0".5	ATCA	[76]

The errors in parentheses refer to R.A. and DEC separately, whereas those that appear in the column “Error” refer to both coordinates.

3.1 SAX J1808.4–3658

The source SAX J1808.4–3658 was discovered with the X-ray satellite *BeppoSAX* during an outburst in September 1996 [77]. The source showed via three type I X-ray bursts that the compact object in the binary is a NS. The 2–28 keV peak luminosity of $3 \times 10^{36} \text{ erg s}^{-1}$ [78] is rather faint and below the average peak luminosity reached by other LMXBs. X-ray pulsations were not detected during this outburst, with poorly constraining upper limits of 20% on the pulsed fraction. Coherent pulsations at 401 Hz were discovered instead in 1998, during the second observed outburst [8], thanks to the better sensitivity of the Proportional Counter Array (PCA) on *RXTE*. An orbital modulation of 2.01 hr was detected using Doppler delays in the coherent timing data [79] and it was suggested that the companion of the pulsar is a heated brown dwarf with mass of $\approx 0.05 M_{\odot}$ [80]. No thermonuclear X-ray bursts were observed during the 1998 outburst, but re-analysis of the 1996 data provided marginal evidence for burst oscillations at the NS spin frequency [78].

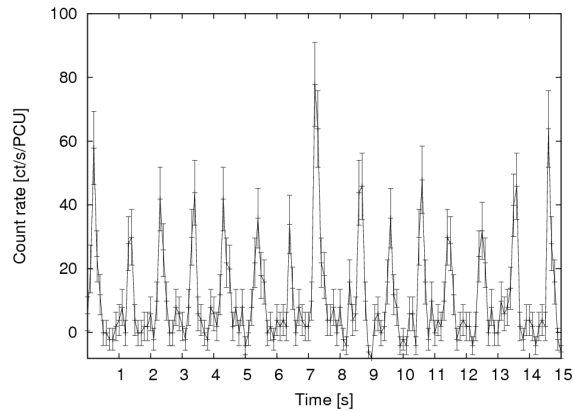
SAX J1808.4–3658 went into outburst again in 2000, 2002, 2005, 2008 and 2011, with an approximate recurrence time of about 1.6–3.3 yr, and is the best sampled and studied of all AMXPs. All of the outbursts showed faint luminosities, with peaks always below $10^{37} \text{ erg s}^{-1}$, even when considering broad energy bands. The 2000 outburst was poorly sampled due to solar constraints, and was observed only during the “flaring tail”, a peculiar outburst phase displayed by only a very small number of X-ray sources. The typical SAX J1808.4–3658 outburst can be split in five phases: a fast rise, with a steep increase in luminosity lasting only a few days, a peak, a slow decay stage, a fast decay phase and the flaring tail. The first four phases are typical of several X-ray binaries and dwarf novae and can in principle be partially explained with the disk instability model. The flaring tail instead shows bumps, called

“reflares”, with a quasi-oscillatory behaviour of a few days and a variation in luminosity of up to three orders of magnitude on timescales ~ 1 -2 days [81, 82, 83]. The flaring tail has no clear explanation within the disk instability model [84], but has been observed in all outbursts [83, 85]. Pulsations are still detected during this low luminosity stage, and a strong ~ 1 Hz oscillation is observed to modulate the reflares (see Figure 1; [86, 83]). This has been interpreted as a possible signature of the onset of a disk instability with radial perturbation of the magnetospheric boundary (the so-called “Spruit and Taam instability” [87, 88]) close to the onset of the “propeller stage” [83]. The 1 Hz modulation, however, has not appeared in all the flaring tails of the different outbursts, but only in the years 2000, 2002 and 2005. The presence of the 1 Hz modulation during the 1998 flaring tail cannot be excluded, however, due to lack of observations.

The study of the high frequency aperiodic variability of SAX J1808.4–3658 led to a breakthrough when twin kHz Quasi Periodic Oscillations (QPOs) at a frequency of approximately 500 and 700 Hz were discovered for the first time in a source with a well established spin frequency [89]. The twin kHz QPOs (Section 8) were observed when SAX J1808.4–3658 reached the peak luminosity during the 2002 outburst, and their frequency separation of 196 ± 4 Hz is consistent with being at half the spin frequency. This suggested a possible link between spin frequency and kHz QPOs and hence refuted the beat-frequency model for the formation of kHz QPOs. In this model the upper kHz QPO at 700 Hz reflects an orbital frequency in the inner accretion disk, whereas the lower kHz QPO should appear as a beat frequency between the upper kHz QPO and the spin frequency. The twin kHz QPOs must be separated by a frequency equal to the spin frequency and not half its value, as observed. The upper kHz QPO was observed during most of the outburst, and another QPO at 410 Hz also appeared during a few observations [89]. The origin of this latter QPO is unclear and it has been suggested [89] that it might be related to the side-band phenomenon observed in other LMXBs [90]. In particular, it was suggested that the 410 Hz QPO might be a sideband of the pulsation, created by a resonance occurring at the radius in the disk where the general relativistic vertical epicyclic frequency matches the spin frequency of the pulsar.

The 3-150 keV X-ray spectrum of the 1998 outburst had a remarkably stable power law shape with photon index of ~ 2 and a high energy cutoff at ~ 100 keV [91]. Further spectral analysis provided evidence for a two-component model: a blackbody at soft energies and a hard Comptonization component at higher energies [92]. The blackbody is interpreted as the heated hot spot on the NS surface, whereas the Comptonization is produced in the accretion shock created at the bottom of the magnetic field lines as the plasma abruptly decelerates close to the NS surface. The presence of an accretion disk was detected much later at lower energies, with observations taken in 2008 with the EPIC-pn camera on the *XMM-Newton* telescope. Its large sensitivity at soft energies (down to about 0.5 keV) well below the nominal 2 keV limit of *RXTE*, allowed the detection of the typical cold accretion disk signature at a temperature of 0.2 keV [20, 93]. The signature of a fluorescent relativistic iron $K\alpha$ emission line profile was also found. A similar result was obtained with combined *XMM-Newton* and *Suzaku* data [21]. Spectral modeling of the iron line

Fig. 1 Small portion (15 s) of the 2005 X-ray light-curve of SAX J1808.4–3658, showing the 1 Hz flaring phenomenon during a reflare. The amplitude of the 1 Hz oscillation reaches 125% rms (Figure from [83]).



constrained the magnetic field of the pulsar to be $\sim 3 \times 10^8$ G at the poles [21, 20]. Simultaneous spectral modeling of the inner disk radius and pulse profile shapes of the 2002 outburst [94] lead to a similar constraint of the magnetic field ($B \sim 10^8$ G).

Thermonuclear bursts were observed in 1996, 2002, 2005, 2008 and 2011 [78, 95, 85]. Most of the bursts exhibit photospheric radius expansion (PRE), where the luminosity reaches the Eddington limit, lifting the photosphere off the surface of the NS until the flux dies down. Such bursts can be used as standard candles [96]. The distance estimated using this method is 2.5–3.6 kpc [85, 78]. Note that a different lower limit of 3.4 kpc is reported in [85]. This lower limit is based on the assumption that the long-term mass transfer rate is driven purely by loss of angular momentum in the binary via emission of gravitational radiation, which may not be a good approximation (see Section 6). All bursts observed in the *RXTE* era have shown burst oscillations (with a possible marginal detection in one burst in 1996 observed with *BeppoSAX*) with an amplitude of a few percent rms. SAX J1808.4–3658 provided the first robust confirmation that burst oscillation frequency was, to within a few Hz, the spin frequency of the star ([95] and Figure 2).

An optical/IR counterpart (V4584 Sagittarii) was discovered during the 1998 outburst, coincident with the position of SAX J1808.4–3658 [97]. The reported magnitudes of the candidate were $V = 16.6$, $R = 16.1$, $I = 15.6$, $J = 15.0$, $H = 14.4$, $K = 13.8$, with an uncertainty of 0.2 mag in VRI and < 0.1 mag in JHK. The V band was further monitored [98] and a possible sinusoidal modulation at the 2 hr period of the binary identified, together with a decay in the luminosity as the outburst progressed in its decay stage. A multiband optical/IR photometric study of the optical counterpart during the 1998 outburst revealed an optical flux consistent with an X-ray heated accretion disk and an inclination of $\cos i = 0.65^{+0.23}_{-0.33}$ (90% c.l.) [99]. The IR observations, however, showed an excess with respect to an accretion disk plus irradiated donor star model. This excess was transient in nature, as it was detected only during one observation, the rest being consistent with the irradiated accretion disk plus donor star model. Radio observations carried out one week later (April 27, 1998) with the Australia Telescope Compact Array (ATCA) revealed a transient

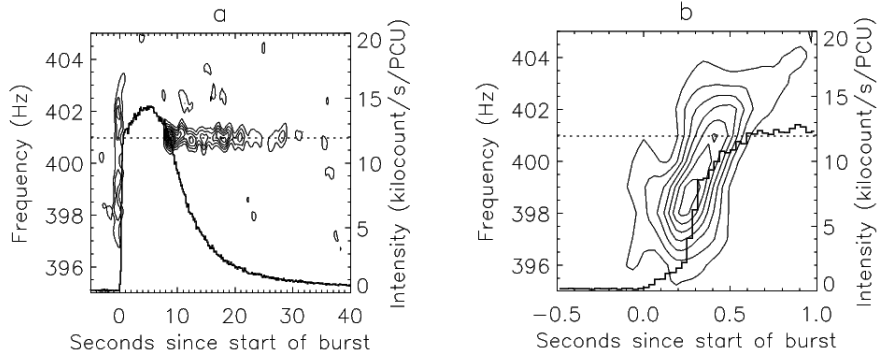


Fig. 2 **Left panel:** a typical X-ray burst observed in the 2-60 keV energy band on 18 October 2002 with a dynamical power spectrum of barycentered data superimposed. The contours refer to power levels of 2 s power spectra spaced by 0.25 s. The burst oscillations are clearly detected during the rise, overshooting the spin frequency of SAX J1808.4-3658 at 401 Hz. The oscillations then disappear during the photospheric radius expansion close to the burst peak and reappear in the burst tail at a frequency consistent with the 401 Hz of the pulsar. **Right panel:** a zoom in of the burst rise and peak, with finer power spectra resolution of 0.25 s spaced by 0.03125 s. The frequency overshoot is clearly visible, with the BO frequency reaching ~ 403 Hz (Figure from [95]).

radio counterpart with a flux of ~ 0.8 mJy with no further detection at later epochs during the 1998 outburst or during quiescence. This observation was interpreted as synchrotron emission which might in principle constitute a viable explanation also for the IR transient excess. This suggests that material can be ejected from the binary via relativistic jets and/or outflows. A similar IR excess was detected during 2005 June 5 [100] and radio Very Large Array (VLA) observations carried at 4.86 and 8.46 GHz showed a transient ~ 0.4 mJy flux, again interpreted as possible synchrotron emission [101].

Optical observations in *quiescence* have been performed extensively for over a decade [102, 103, 104]. In the first observation, a clear optical excess was detected, well above the level expected from residual X-ray irradiation of the donor star that is still present during quiescence [102]. A clear modulation at the orbital period of the binary in IR bands was also identified [103, 105, 104]. To explain the observations, a strong source of extra irradiation was required. In particular, the initial donor mass estimate of $0.05 M_{\odot}$ [80] was revised to 0.07 - $0.11 M_{\odot}$, to account for the large entropy of the donor in quiescence [103]. The optical excess was first interpreted as evidence for the turning on of an active radio pulsar when accretion halts [106, 107]. Whether this is the correct interpretation is still to be verified, but it appears a plausible explanation even though no radio pulsations have been detected [108].

3.2 XTE J1751–305

The AMXP XTE J1751–305 was discovered by *RXTE* on April 3, 2002 and coherent pulsations at 435 Hz were observed immediately [22]. The orbital period of 42 minutes makes this AMXP an ultra-compact binary with a heated He or C/O white dwarf of minimum donor mass $0.013\text{--}0.017 M_{\odot}$ ² (depending on the NS mass) [15]. Archival observations taken with the All-Sky-Monitor (ASM) aboard *RXTE* showed that a faint outburst had already occurred in 1998. Three other outbursts were observed in 2005, 2007 and 2009. The first two had very faint peak luminosities of about 10%–20% the value reached in 2002. The 2005 outburst in particular was observed by *INTEGRAL* [110] and lasted only 2 days, with only one follow-up *RXTE* observation [111]. No high resolution timing data were taken, and the association of the outburst with XTE J1751–305 remains dubious given the large source position error of the two X-ray observatories. On April 5, 2007, XTE J1751–305 was observed with *RXTE* during routine galactic bulge monitoring observations [112]. No pulsations were seen because of the dim flux (10 mCrab in the 2–10 keV) and the short bulge scan exposure (~ 50 s). However, a follow-up *Swift* observation made the identification of the source certain thanks to the high angular resolution of the XRT telescope [113]. The outburst had a fluence of about 10^{-4} erg cm⁻², comparable to the already low 2002 outburst fluence of 2.5×10^{-3} erg cm⁻² [22]. In 2009 *INTEGRAL* recorded a new outburst [114] and *RXTE* observed it extensively, with pulsations immediately detected [115]. This outburst has a duration and brightness similar to the 2002 event.

XTE J1751–305 shows no Type I X-ray bursts and its distance is therefore difficult to determine. The X-ray spectrum taken with *XMM-Newton* in 2002 showed a power law with spectral index 1.44 ± 0.01 contributing 83% of the total 0.5–10.0 keV flux and a blackbody at temperature $kT = 1.05 \pm 0.01$ keV [116]. A broadband spectrum analysis of the 2002 outburst was performed by combining *RXTE* (PCA and HEXTE) and *XMM-Newton* (EPIC-pn) data [117]. The analysis revealed the presence of three components, two blackbodies and a hard component, which were interpreted as a thermal emission from a cold accretion disk ($kT \sim 0.6$ keV), a hotter ($kT \sim 1$ keV) hot spot on the NS surface and a thermal Comptonization in plasma of temperature $kT \sim 40$ keV (see Fig 3). These findings were very similar to the spectral modeling described above for SAX J1808.4–3658. Unsuccessful searches for an optical/near IR counterpart were carried out during the 2002 outburst and in quiescence [118]. However the upper limits are not particularly constraining if one assumes that the source is close to the Galactic center ($d = 8.5$ kpc).

² Hydrogen rich donor stars never reach orbital periods below ~ 80 min [109]

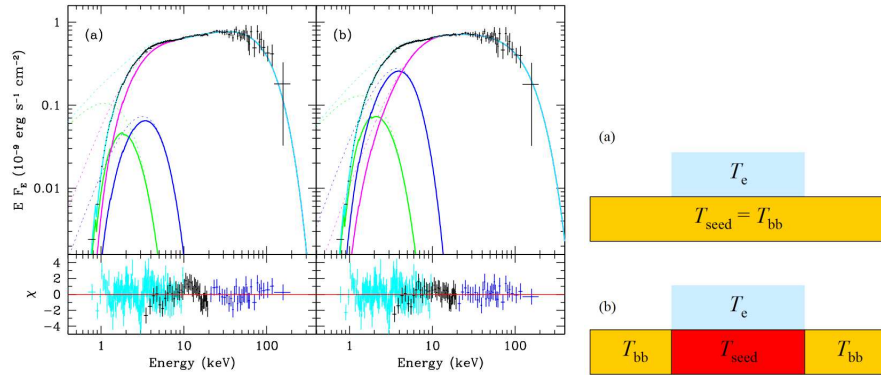


Fig. 3 Broadband X-ray spectrum of XTE J1751–305 obtained by combining *XMM-Newton* (light blue points) and *RXTE* data (black and dark blue points). Three components are used to model the spectrum: a cold blackbody identified with the thermal disk emission (green line), a hot blackbody (hot spot; blue line) and a hard tail created via thermal Comptonization in a plasma (pink line). The left spectrum refers to the emission geometry “(a)” in which a small temperature gradient is present in the hot spot. The right spectrum uses the “(b)” model, with a large temperature gradient between the hot spot and the remaining illuminated NS surface around the accretion shock (image taken from [117])

3.3 XTE J0929–314

With a spin of 185 Hz and an orbital period of 43.6 min, XTE J0929–314 was the third AMXP to be discovered, and the second in an ultra-compact binary. The source was first detected on April 13, 2002 by the *RXTE*/ASM [119]. Coherent pulsations were first detected in an observation performed on May 2, 2002 [24]. Doppler modulation of the pulsations revealed the ultra-compact nature of the binary [25]. The very small mass function ($2.7 \times 10^{-7} M_{\odot}$) implied a tiny donor star of minimum mass of about $0.01 M_{\odot}$. This requires a cold He white dwarf companion with a possible H-rich envelope that would explain the detection of an H_{α} line at $\lambda = 6,563 \text{ \AA}$ [120] during the 2002 outburst. The 2002 outburst lasted at least 52 days, but only 34 days were monitored by the high time resolution *RXTE*/PCA instrument. The X-ray spectrum of XTE J0929–314, taken with *Chandra*, showed a power-law plus blackbody similar to XTE J1751-305 [121].

XTE J0929–314 has been detected in several wavebands: radio, near IR and optical counterparts were identified during the 2002 outburst. An optical counterpart consistent with the position of XTE J0929–314 was detected in V, B, R and I bands [122]. Broad band BVRI observations at the Mt Canopus 1-m telescope carried in May 2002 revealed a modulation of $\approx 10\%$ in the I band with periodicity consistent with the orbit of the binary [68]. An anomalous I-band excess was also observed in the first few days of the outburst and was interpreted as synchrotron radiation, in addition to the accretion disk/irradiated donor emission. This behavior is similar to that reported for SAX J1808.4–3658. The optical spectrum of the source (in

outburst) shows a strong emission line at $4,640 \text{ \AA}$ compatible with a C/O or a He/N disc [123]. Optical spectroscopy also lead to the conclusion that the most likely donor of XTE J0929–314 is a C/O white dwarf. A radio counterpart (during the outburst) was detected with the VLA at 4.86 GHz [124]. A source flux of 0.31 ± 0.07 mJy (May 3) and 0.36 ± 0.05 mJy (May 7) was reported from a position only 0.8 arcseconds from the previously detected optical position [122]. The source has also a very faint optical counterpart ($R = 27.2$) in quiescence [125]. PSF *VRI* photometry in quiescence [126] also suggested that the donor is irradiated by a source which emits in excess (by a factor of ≈ 8) of the quiescent X-ray luminosity of XTE J0929–314 ($L_X \sim 4.5 \times 10^{31} \text{ erg s}^{-1}$).

3.4 XTE J1807–294

The fourth AMXP was discovered on February 21, 2003 by *RXTE* [26]. The source is the third ultra-compact AMXP, with the shortest orbital period known to date, 40.1 min, and a minimum companion mass of $0.0066 M_\odot$. Simultaneous *INTEGRAL*, *XMM-Newton* and *RXTE* spectral analysis [127] constrains the companion mass to be less than $0.022 M_\odot$, implying that the donor is likely a C/O white dwarf rather than a He white dwarf, which would require unlikely a-priori low inclinations. With the exception of the quasi-persistent intermittent AMXP HETE J1900.1-2455, XTE J1807–294 had the longest AMXP outburst observed so far: ≈ 120 days, of which ≈ 109 days had sufficiently high flux to allow the detection of pulsations. Twin kHz QPOs were detected in several observations and the separation $\Delta \nu$ of the kHz QPOs is consistent with the spin frequency of the AMXP [128]. No counterparts have been reported at any wavelength during either outburst or quiescence. A candidate optical counterpart detection was reported in 2009 [126] with $V \sim 22.1$ and $R \sim 21.4$ along with a tentative detection in the *J* band. The counterpart falls within the $0''.6$ *Chandra* (90% confidence level) error circle. No variability has been observed, with upper limits of 0.1 mag.

3.5 XTE J1814–338

The fifth AMXP was found during routine Galactic center observations by the *RXTE/PCA* on June 5, 2003 [31]. The pulse frequency is 314 Hz and the orbital period 4.3 hr, giving a minimum companion mass of $0.17 M_\odot$. The outburst lasted for ≈ 50 days and pulsations were detectable for ≈ 45 days. The source showed 28 Type I X-ray bursts and *RXTE* detected burst oscillations at the spin frequency in all bursts. The 28th burst showed signs of PRE, allowing a determination of the source distance of ≈ 8 kpc. The X-ray position of XTE J1814–338 is consistent with the *EXOSAT* source EXMS B1810-337, detected in September 1984 [129]. If this identification is correct, then XTE J1814–338 has a recurrence time of ~ 20 yr.

The optical counterpart was first tentatively identified using BVRI data taken with the Magellan 6.5 m telescope [130]. An observation of H and He emission lines, with a double-peaked H_α line typical of interacting binaries, was reported soon after the discovery of the binary [131]. The counterpart was studied in more detail and finally unambiguously identified [67]. The B, V and R counterparts during the 2003 outburst had magnitudes between 18 and 19 mag, whereas the I band was observed with an excess flux reaching about 17.4 mag. This excess is again similar to that reported for SAX J1808.4–3658 and XTE J0929–314 and suggests the presence of jets and/or outflows. A faint object with $V \sim 23.3$ and $R \sim 22.5$ was identified in ESO Very Large Telescope (VLT) archival data taken in May 20–21, 2004 [126]. A multiband Very Large Telescope (VLT) campaign carried in 2009 (during quiescence) shows an irradiated companion star that requires an energy source compatible with the spin-down luminosity of a millisecond pulsar [132]. This proves further evidence that AMXPs might turn on as radio pulsars when in quiescence.

3.6 IGR J00291+5934

IGR J00291+5934 is the fastest AMXP known, with a spin of 599 Hz. The source was discovered by *INTEGRAL* on 2004 December 2 [133] and prolonged *RXTE* observations lead to the discovery of pulsations [134] and an orbital period of 2.46 hr, with a minimum donor mass of about $0.04 M_\odot$ [135]. The 2004 outburst had a duration of ≈ 14 days from the *INTEGRAL* discovery, with a smooth flux decay. On 2008 August 13 the source started a new outburst [136] and was observed for about a week before reaching an X-ray flux level below the sensitivity limit of *RXTE*. The peak flux observed was about half the value reached in 2004. Follow up *Swift*/XRT observations on August 21 revealed a flux level below $10^{-11} - 10^{-12} \text{ erg s}^{-1}$ and an *XMM-Newton* observation on August 25 provided a 2–10 keV flux of $(1.4 \pm 0.3) \times 10^{-14} \text{ erg s}^{-1}$ [137], compatible with the $10^{-13} \text{ erg s}^{-1}$ (0.5–10 keV) quiescent flux level observed two months after the end of the 2004 outburst [138]. On 2008 September 21, the source re-brightened again, showing another outburst lasting for about 14 days. The fluence of the second and third outbursts were very similar and it is unclear whether the two 2008 outbursts were distinct [37] or part of the same outburst. An analysis of archival *RXTE*/ASM data revealed possible outbursts in 1998 November and 2001 September, suggesting a recurrence time of 3–4 yr [139].

The pulsar has shown no thermonuclear bursts despite very similar orbital parameters to SAX J1808.4–3658. The donor star of IGR J00291+5934 is also probably a X-ray heated brown dwarf as in SAX J1808.4–3658 [33]. Broadband spectral observations performed during the 2004 outburst with *INTEGRAL* and *RXTE* were well fitted with a thermal Comptonization model with an electron temperature of 50 keV and Thomson optical depth $\tau_T \sim 1$ in a slab geometry [34]. The *RXTE* data analysis of the first 12 days of the outburst revealed a power law plus blackbody (with $kT \sim 1 \text{ keV}$) interpreted as emission from the hot spot on the NS surface. Fur-

ther simultaneous *RXTE* and *Chandra*/HETGS (High Energy Transmission Grating Spectrometer) spectral observations collected towards the end of the 2004 outburst revealed a power law plus a cold black body at 0.42 keV, interpreted as the cold accretion disk, with no signature of the hot spot blackbody [140]. This is consistent with the lack of detected pulsations towards the end of the outburst [33].

A tentative optical counterpart was identified during the 2004 outburst [141], with an R magnitude of 17.4. Follow up spectral measurements with the 4.2-m William Herschel Telescope on La Palma strengthened the association with the identification of a weak HeII and H_α line [142]. An optical/NIR photometric study in quiescence was then performed in 2005 with the 3.6-m Telescopio Nazionale Galileo (TNG) [143]. The VRIJH counterparts of IGR J00291+5934 were detected, with a strong upper limit in the K-band. The optical light curve shows variability consistent with the 2.46 hr orbital period. The radio to X-ray Spectral Energy Distributions (SEDs) revealed a blue component indicative of an irradiated disc [137]. The SED contained also a transient NIR excess similar to that found in SAX J1808.4–3658, XTE J0929–314 and XTE J1814–338. An H_α line was observed in the optical spectrum of the 2004 and 2008 outbursts. Evidence was also found for an *I* band excess during quiescence in an observation performed with the 4.2-m William Herschel Telescope (WHT) on 2006 September 13 and 14 [138].

Radio observations taken on 2004 December 4 with the Ryle Telescope in Cambridge at 15 GHz resulted in a detection at 1.1 mJy [144]. Follow up observations taken one day later gave a non detection, with upper limits of 0.6 mJy at 15 GHz [145]. The Westerbork Synthesis Radio Telescope (WSRT) observed IGR J00291+5934 between 2004 December 6 and 7, and a radio counterpart was seen at 5 GHz with a flux of 0.250 ± 0.035 mJy [145]. Very Large Array (VLA) observations performed on 2004 December 9 at 4.86 GHz confirmed the reported radio detection, with a flux of 0.17 ± 0.05 mJy. The source was not detected in radio during the 2008 outburst, with upper limits of 0.16 mJy at 5 GHz in an observation taken between August 15 and 16 [146].

3.7 HETE J1900.1–2455

The *High Energy Transient Explorer* (HETE–2) discovered HETE J1900.1–2455 on 2005 June 14 via an X-ray burst [147]. Follow up observations taken on June 16 by *RXTE*/PCA showed pulsations at 377 Hz [148]. A source distance ~ 4 –5 kpc (assuming a typical NS mass of $1.4M_\odot$ and a He rich NS atmosphere) was determined using the first type I X-ray burst detected with HETE–2 [149, 150], which showed PRE. The orbital period was determined to be 1.4 hr with a minimum companion mass of $0.016M_\odot$ [39]. Unlike the other AMXPs with brown dwarf companions discussed so far, the donor star in HETE J1900.1–2455 is most likely a brown dwarf which does not require X-ray irradiation or a non-standard evolution to fill its Roche lobe.

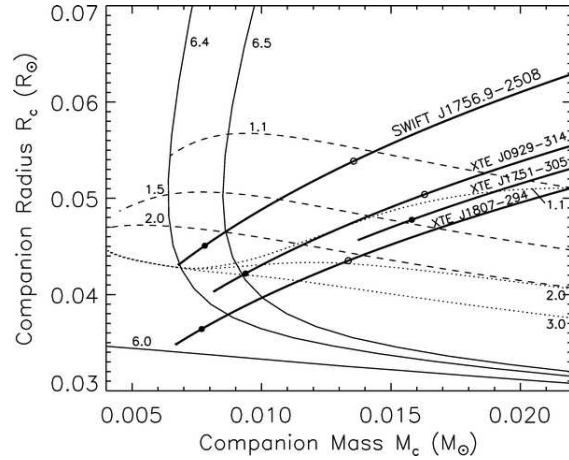
A single 882.8 Hz QPO was detected in the *RXTE* lightcurve during a bright flare occurred on MJD 53,559.45 [39]. Simultaneous *RXTE* and *INTEGRAL* observations showed that the 2–300 keV spectrum is well fit by a blackbody component peaking at 0.8 keV plus thermal Comptonization with electron temperature of 30 keV and optical depth $\tau_T \sim 2$ for a slab geometry [151]. The source was detected up to energies of 200 keV and the 0.1–200 keV luminosity was inferred to be $5 \times 10^{36} \text{ erg s}^{-1}$. Although the peak luminosity is not particularly high compared to other AMXPs, the average mass accretion rate $\langle \dot{M} \rangle$ of HETE J1900.1–2455 is among the highest observed due to its prolonged X-ray outburst that has lasted for eight years (and is still active as of November 2013) [152, 153]. This makes HETE J1900.1–2455 a so called “quasi-persistent source”, i.e., an X-ray binary with a prolonged outburst duration of several years. Despite the long baseline provided by the outburst, pulsations were *continuously* detected only in the first two months of the observations although sporadic pulse detections occurred over a baseline of about 2.5 yrs (Section 2.1).

An optical counterpart was identified with the Robotic Palomar 60-inch Telescope on June 18 [75]. The source had a brightness $R \sim 18.4$. Near IR observations taken with the 1.3 m robotic PAIRITEL telescope on Mt. Hopkins indicated a counterpart with $J = 17.6 \pm 0.2$, with no variability between observations taken on June 16 and 18 [154]. The counterpart was observed again with the FLWO 1.2-m telescope at Mt. Hopkins with $V = 18.09 \pm 0.03$, $R = 18.02 \pm 0.03$ and $I = 17.88 \pm 0.02$ [155]. A spectral analysis of the optical counterpart showed a HeII 4,686 Å, suggesting correct identification of the binary’s optical counterpart. Further optical observations taken with the 8.4-m Large Binocular Telescope (LBT) on Mt. Graham, Arizona, showed a brightness of $R = 18.64 \pm 0.02$ and 18.54 ± 0.02 on 2007 June 13, after an initial decline of 1.7 mag in optical, and a non-detection in X-rays which occurred two weeks prior [156, 157]. Phase resolved optical photometry and spectroscopy obtained in September 2006 at the 2.3-m ATT, 3.5-m WIYN and 8.4-m LBT [158], revealed a sinusoidal modulation in the R-band, close to the orbital period. However, further analysis showed that the modulation is probably due to a super-hump of a precessing accretion disk, and not irradiation of the donor star. A broad H_α emission line in a 10-m Keck I spectrum taken by the same authors confirmed this interpretation. No radio counterpart was identified in VLA observations on 2005 June 19 and 24 at 8.46 GHz [159].

3.8 *Swift* J1756.9–2508

Swift J1756.9–2508 was discovered by the Burst Alert Telescope (BAT) aboard *Swift* on June 7, 2007 [40]. High time resolution data from the *RXTE*/PCA, showed that the source was a 182 Hz AMXP [160]. This was the fourth ultra-compact AMXP discovered, with an orbital period of 54.7 min. The minimum donor star mass, given by the X-ray mass function, is $0.0067 M_\odot$. It has been proposed that *Swift* J1756.9–2508 harbors a He rich white dwarf which is irradiated by X-ray

Fig. 4 Mass-Radius relation (solid line) for the companions of the four ultra-compact AMXPs, as determined from the mass function. Open and filled circles indicate an inclination of 60° and 30° , respectively. Dotted and dashed curves are non-irradiated/irradiated white dwarf models, respectively. The numbers next to the curves indicate the degeneracy parameter. The solid thin curves are pure C white dwarf models and the numbers refer to the log of the temperature (in Kelvin). (Figure from [40])



flux from the accretor (see Figure 4 and [40]). The spectrum of the source, taken with *Swift*/XRT, BAT and *RXTE*/PCA, is well fit by a single absorbed power law with spectral index $\Gamma \sim 2$ [40]. The 2007 outburst length was 13 days, with no prior outbursts seen in archival data. A second outburst was detected on 2009 July 8 by *Swift*/BAT and *RXTE*/PCA [161]. This second outburst showed a very similar length and shape as the 2007 outburst. No thermonuclear bursts were observed. There is evidence for a fluorescent Fe line in the X-ray spectrum, although the poor spectral resolution of *RXTE* prevented to constrain the physical parameters of the system [41]. A possible NIR K_s counterpart was identified [162] by inspecting the variability of 70 objects within the 3.5 arcsec error circle of the *Swift*/XRT position. The candidate counterpart exhibited variability of about 1.3 mag in two observations taken close to the end of the outburst (2007 June 19) and during quiescence (2007 July 1). No radio counterpart has been identified [163, 164] and Chandra observations taken on 2007 July 7 detected one single photon in a 11 ks long observations [165].

3.9 *Aql X-1*

Aql X-1 is perhaps the most peculiar AMXP since it has showed pulsations at 550.27 Hz in just 120 s of X-ray data [42]: the short baseline means that no coherent timing solution can be obtained. As a consequence, no orbital modulation or mass function has yet been measured with X-rays. The source shows thermonuclear bursts with burst oscillations whose asymptotic frequency is ≈ 0.5 Hz smaller than the coherent accretion powered pulsations observed in 1998 [166]. The recurrence time of the outbursts is about 1 yr and they have been extensively monitored at different wavelengths. Twin kHz QPOs were observed at a frequency of ~ 800 and ~ 1080 Hz [167], so that their frequency separation is consistent with being equal to half

the NS spin frequency. The optical counterpart of Aql X-1, named V1333 Aql, was identified in 1978 [168] as a star with $B \sim 17$ mag (in outburst) and $B > 20$ mag (in quiescence). The spectral type of the source was identified as a K6-M0 star [169]. An orbital modulation at a period of 18.95 hr was reported from an optical modulation of the counterpart of Aql X-1 [170, 43]. Despite several attempts, the radio counterpart has been observed in only a few outbursts at a level of $\sim 0.1 - 0.5$ mJy [171, 172, 173]. In November 2009, radio observations provided evidence for the emission to arise from steady jets triggered at state transitions from the soft to hard state [174].

3.10 SAX J1748.9–2021

SAX J1748.9–2021 was discovered with the *BeppoSAX*/WFC on August 22, 1998 in the globular cluster NGC 6440 [175, 176]. The distance of the source is well constrained thanks to the knowledge of the globular cluster distance of 8.5 ± 0.4 kpc [177]. *RXTE*/PCA and *BeppoSAX*/WFC monitoring revealed no pulsations, but thermonuclear bursts were observed with no burst oscillations. The position of the source was coincident with the position of MX 1746-20 detected by *Uhuru* and *OSO-7* in 1971-1972. However, given the large error box of these missions, it is not possible to establish a secure association between the two sources. SAX J1748.9–2021 showed a typical average X-ray spectrum with a power-law with photon index 1.5 and a soft blackbody component at $kT = 0.9$ keV [175]. However, other spectral models also gave a good fit to the data [175].

In August 2001, after 3 years of quiescence, SAX J1748.9–2021 started a new outburst observed with the *RXTE*/ASM. *Chandra* observations allowed the establishment of a precise position in the globular cluster and confirmed that the 1998 outburst was from the same source. Thermonuclear bursts without burst oscillations were again observed. The beginning of the third outburst was detected in 2005 March 7 during a routinely *RXTE*/PCA Galactic Bulge Scan Survey. The source was monitored until 2005 July 21 and several pointed *RXTE*/PCA observations were performed. The first pulsations reported for this source were seen in the 2005 outburst [178, 179]. A coherent signal at $\simeq 442$ Hz was detected during a flux decay reminiscent of the tail of a superburst. However, neither the temporal profile nor the energetics of the tail were consistent with a super-burst and this led to the suggestion that this was a new intermittent AMXP [179]. An independent analysis of *RXTE*/PCA archival data from the 2001 and 2005 outburst revealed intermittent coherent X-ray pulsations at 442 Hz, appearing and disappearing on timescales of few hundred seconds [44, 45]. A further outburst was observed in December 2009 with *RXTE* and intermittent pulsations were observed again [65]. Observations in quiescence carried out in July 2000 and June 2003 revealed an X-ray spectrum with a thermal component detected in both observations. The 2000 observation, however, required also a power law component possibly because of residual accretion on the NS [180].

Thanks to *ROSAT*/HRI archival observations and a 3.5 m New Technology Telescope (NTT) observation on 1998 August 26–27, two candidate optical counterparts, dubbed V1 and V2, were identified [176]. V2, with $B \simeq 22.7$ mag, has now been recognized as the true counterpart thanks to the precise astrometric position obtained with the 2001 *Chandra* observations [181]. VLA radio observations provided stringent upper limits during the 2009 outburst and implied that the radio emission is quenched at high X-ray luminosities [182].

3.11 NGC 6440 X-2

On 2009 June 28, the X-ray transient NGC 6440 X-2 was discovered [183] in a *Chandra* observation of the globular cluster NGC 6440 (the same cluster that harbors the AMXP SAX J1748.9–2021). Coherent pulsations at 206 Hz were detected in a subsequent outburst in *RXTE*/PCA observations on 2009 August 30 [46]. The orbital period is 0.95 hr, making this the fifth ultra-compact AMXP discovered. One of the most striking features of this pulsar is the very low long-term average mass accretion rate $\langle \dot{M} \rangle < 2 \times 10^{-12} M_{\odot} \text{ yr}^{-1}$, which could be determined thanks to the well-defined distance to the globular cluster [71]. Peak flux is one of the faintest observed from the AMXPs ($L_{2-10\text{keV}} < 1.5 \times 10^{36} \text{ erg s}^{-1}$) and the outburst length is extremely short, with a duration of $\approx 3\text{--}5$ days. It should be noted that the *RXTE*/PCA Galactic Bulge Scan flux limit corresponds to a luminosity $\sim 10^{35} \text{ erg s}^{-1}$ [46] so that the presence of a longer and very faint outburst cannot be ruled out, although archival *Chandra* observations did not reveal any counterpart in quiescence with an upper limit on the X-ray luminosity of $L_X \lesssim 10^{31} \text{ erg s}^{-1}$. This raises the question of how many faint sources of this kind might have been missed, particularly important given that AMXPs seem to be associated with faint LMXBs, and systems of this type may therefore contain undiscovered AMXPs.

The recurrence time of the outburst is also the shortest among AMXPs, \sim one month. An *RXTE*/PCA and *Swift*/XRT monitoring campaign revealed the occurrence of 10 outbursts between 2009 and 2011 [71, 184]). In November 2009, visibility constraints and a new outburst of the other AMXP SAX J1748.9–2021 prevented further observations of NGC 6440 X-2. A strong ($\sim 50\%$ rms) 1 Hz modulation was observed in the light-curve of at least 6 outbursts [184], which strongly resembled the 1 Hz modulation seen in SAX J1808.4–3658 [86, 83].

Despite the precise astrometric X-ray position of the source, the optical counterpart of NGC 6440 X-2 has not yet been identified, with $B > 22$ and $V > 21$ from archival *Hubble Space Telescope* (HST) imaging of the globular cluster when NGC 6440 X-2 was in quiescence. During the 2009 August outburst, Gemini-South observations did not reveal any counterpart with $g' > 22$. Observations carried with the CTIO 4-m telescope during the 2009 July outburst also did not reveal any counterpart with $J > 18.5$ and $K > 17$ [71].

3.12 IGR J17511–3057

The X-ray binary IGR J17511–3057 was discovered during Galactic Bulge Monitoring by the *INTEGRAL* satellite in 2009 September 12 [185]. Coherent pulsations at 245 Hz and an orbital modulation of 3.5 hr were measured with follow up observations by the *RXTE/PCA* [47]. Given the X-ray mass function, the minimum donor star mass is $0.13 M_{\odot}$. The X-ray light-curve was also extensively monitored by *Swift/XRT*, *XMM-Newton*, *RXTE/PCA* and *Chandra*. The light-curve showed a typical fast rise with a slow decay lasting for about 20 days, before entering a fast decay phase [186, 187]. Curiously, while the source was in the fast decay phase, a very short and faint outburst of the ultra-compact AMXP XTE J1751–305 appeared in the same field of view (FoV) of *RXTE*. The mini-outburst of XTE J1751–305 lasted less than 3 days, and pulsations were clearly visible at 435 Hz [115]. Thermonuclear bursts were observed in IGR J17511–3057 with *Swift* [188], and burst oscillations were detected in *RXTE* data [189, 187]. None of the bursts showed PRE, so there are several different distance determinations in the literature. The most constraining gives an upper limit on distance of $\lesssim 5$ kpc [187].

Swift spectral analysis revealed a power law ($\Gamma \sim 2$) plus a blackbody at 0.9 keV [188]. Broadband spectral data from simultaneous *RXTE/PCA* and *Swift/XRT* observations could be well fitted with a three model component [190]: a disk with low temperature ($kT \sim 0.24$ keV), a hot black body (hot spot with $kT \sim 1$ keV) and a Comptonization component originating from the accretion shock (electron temperature $T_e \sim 30$ keV; $\tau_T \sim 2$). The spectral fitting also required a fluorescent iron line at 6.4 keV with Compton reflection and provided an interstellar absorption column of $N_H = 0.88^{+0.21}_{-0.24} \times 10^{22} \text{ cm}^{-2}$. Very similar results were obtained using simultaneous *XMM-Newton* and *RXTE/PCA* spectral data [186]. Combined *RXTE/PCA*, *Swift/XRT* and *INTEGRAL* data also gave consistent results using a thermal Comptonization model [191]. Twin kHz QPOs were observed at the beginning and at the end of the outburst, and had $\Delta \nu \simeq 120$ Hz, about half the value of the spin frequency [192]. A NIR counterpart with brightness $K_s = 18.0 \pm 0.1$ was identified with the 6.5 m Magellan Baade telescope on 2009 September 22 [193]. A second observation on October 7, while the X-ray flux was fading rapidly, showed no counterpart with 3σ upper limits of $K_s > 18.8$. No radio counterpart has been found, with upper limits of 0.10 mJy [194].

3.13 Swift J1749.4–2807

The first observation of Swift J1749.4–2807 was made on June 2, 2006 with the *Swift/BAT* telescope, which recorded a high level activity consistent with an unidentified source [195]. This was later identified as a “burst-only” accreting NS binary (i.e., a NS that is bright enough to be detectable only during the occurrence of thermonuclear explosions) thanks to a spectral analysis of the *Swift/BAT* data [196]. The analysis was consistent with the observation of a thermonuclear burst for a

source distance of 6.7 ± 1.3 kpc. Further *Swift*/XRT data analysis revealed an X-ray counterpart of the burst and archival *XMM-Newton* data showed a faint point source coincident with the *Swift*/XRT position [197, 196]. Increased activity was reported in 2010 by *INTEGRAL*, and was linked to the accretion powered emission process [198, 199]. Pulsations were discovered immediately afterwards at 518 Hz in *RXTE*/PCA follow-up observations [200, 49]. A very strong second harmonic was detected at 1036 Hz [201] and orbital modulation was measured at 8.82 hr, giving a minimum donor mass of about $0.6 M_{\odot}$ [202, 203]. *Swift* J1749.4–2807 was finally identified as the first eclipsing AMXP [204] and the inclination of the system was constrained to be $i \sim 74^{\circ} - 78^{\circ}$ [204, 49]. The binary showed three eclipses with a duration of 2172 ± 13 s, allowing the first attempted detection of Shapiro delay effects in X-ray timing data for an object outside the Solar System [204].

To fit the 0.5–40 keV spectrum, an absorption column density of $N_H = 3.0 \times 10^{22} \text{ cm}^{-2}$ and a power-law with spectral index $\Gamma \simeq 1.7$ are required [205]. The absorption column is about 3 times larger than the expected Galactic column density in the direction of the source. The X-ray light-curve showed an exponential decay with a *Swift*/XRT non detection after 11 days since its first 2010 observation. Due to the crowded field (the source is on the Galactic plane), no single counterpart has been identified in NIR counterpart searches [72]. More than forty counterparts were identified in the X-ray error circle with ESO’s Very Large Telescope (VLT).

3.14 IGR J17498–2921

IGR J17498–2921 was discovered by *INTEGRAL* on 2011 August 11 [206]. Soon after, coherent X-ray pulsations were discovered in *RXTE*/PCA data at 401 Hz with an orbital period modulation of 3.8 hr [50]. Type I X-ray bursts were observed with *INTEGRAL* [207] and *RXTE*. Burst oscillations were detected [208, 209] and evidence of PRE placed the source at a distance of 7.6 kpc [208]. *Swift*/XRT observed the source returning to quiescence on 2011 September 19 [210]. A candidate NIR counterpart of IGR J17498–2921 was first detected in archival data taken with the 4-m VISTA telescope at the Paranal observatory [211]. The optical counterpart was detected on 2011 August 25 and 26 with the 2-m Faulkes Telescope South [212]. The position detected was consistent with both the *Chandra* and the NIR counterparts. However, further observations suggested that the NIR/optical counterpart is a foreground star aligned by chance with the X-ray source [213]. This counterpart was confirmed to be a foreground source with observations taken at the 2.5-m Irene du Pont telescope. The analysis suggested that, given the distance and extinction of IGR J17498–2921, the expected magnitudes are $R \sim 28$ and $J \sim 23.3$, both well above the limit reached by the optical/NIR observations [214].

3.15 IGR J18245–2452

The most recent addition to the AMXP family was discovered by INTEGRAL on 2013 March 28 [215] during an X-ray outburst (20–100 keV luminosity of $3 \times 10^{36} \text{ erg s}^{-1}$) and is perhaps the most spectacular of all the AMXPs. The source, at a distance of 5.5. kpc is located in the core of the globular cluster M28 [216]. *XMM-Newton* observations revealed an AMXP whose spin (254 Hz) and orbital parameters were identical to those of a previously known radio millisecond pulsar located in the same region (PSR J1824–2452I, a.k.a. M28I) [12]. This makes this source the first known radio millisecond pulsar that has switched to an AMXP state. The 0.5–10 keV luminosity shows a very peculiar X-ray flickering with flux variations of up to 2 orders of magnitude happening within a few seconds [12, 217]. The two flux states can be described by two very different spectral models with power-law index $\Gamma \sim 1.7$ (high flux) and $\Gamma \sim 0.7$ (low flux) [217]. This has been interpreted as evidence for the onset of a propeller phase *during* the outburst, rapidly alternating with a normal accretion phase [217]. A similar flickering was also observed in quiescence [218] when the source switches from a stable low luminosity state of $\sim 10^{32} \text{ erg s}^{-1}$ to a flickering state with luminosity $\sim 10^{33} - 10^{34} \text{ erg s}^{-1}$.

An iron K_{α} line was also observed in the *XMM-Newton* spectrum [12]. Thermonuclear X-ray bursts were observed by *Swift*/XRT and MAXI [219, 220, 221] and burst oscillations were later identified [222]. Archival optical observations obtained with *HST* revealed a faint counterpart on April 2009 and 2010. However, on August 2009 the *HST* detected a blue counterpart, brighter by ~ 2 mag in several filters (F390W = 20.37 ± 0.06 , F606W = 19.51 ± 0.04 , and F656N = 17.26 ± 0.04) [223, 224], with a strong H_{α} emission indicative of the presence of an accretion disk four years before the 2013 outburst. Radio observations performed with ATCA on 2013 April 5, show a bright radio continuum counterpart (0.62 and 0.75 mJy at 5.5 and 9 GHz, respectively) [76]. The source was last detected in X-rays on 2013 May 1 and soon after it turned back on in radio as a millisecond pulsar [225].

4 Accretion Torques

Once the donor star overflows its Roche lobe, gas flowing through the inner Lagrangian point L_1 carries large specific angular momentum and hence forms an accretion disk around the NS. The type of disk depends on the microphysical conditions governing the gas dynamics [226, 227, 228, 229]. If gas pressure dominates, the disk will be geometrically thin and optically thick [230, 231, 226] with material moving in Keplerian orbits with orbital frequency:

$$v_K = \frac{1}{2\pi} \sqrt{\frac{GM}{R^3}} \simeq 767 \text{ Hz} \left(\frac{M}{1.4 M_{\odot}} \right)^{1/2} \left(\frac{R}{20 \text{ km}} \right)^{-3/2} \quad (1)$$

At a distance of a few tens of kilometers from the NS, the gas orbits several hundred cycles per second and flows almost undisturbed until the magnetic field of the NS (that for AMXPs is of the order of 10^8 G) is strong enough to perturb its orbit. At the magnetospheric-radius r_m , the kinetic energy of the free-falling gas becomes comparable to the magnetic energy of the NS magnetosphere :

$$\begin{aligned} r_m &= \xi r_A = \xi \left(\frac{\mu^4}{2GM\dot{M}^2} \right)^{1/7} \\ &= 35 \text{ km } \xi \left(\frac{\mu}{10^{26} \text{ G cm}^3} \right)^{4/7} \times \left(\frac{\dot{M}}{10^{-10} M_\odot \text{ yr}^{-1}} \right)^{-2/7} \left(\frac{M}{1.4 M_\odot} \right)^{-1/7} \end{aligned} \quad (2)$$

where \dot{M} is the mass accretion rate at the inner disk boundary, μ is the dipole magnetic moment of the NS and r_A is the Alfvén radius. This latter parameter is calculated assuming spherical accretion:

$$\frac{B^2(r_A)}{8\pi} \simeq \frac{1}{2} \rho(r_A) v^2(r_A). \quad (3)$$

The parameters ρ and v are gas density and velocity, respectively. The term $\xi \approx 0.3 - 1.0$ is a correction factor due to the non-spherical geometry of the problem and is required because the gas orbits in a disk rather than falling radially from every direction. In the disk geometry, magnetic and fluid stresses balance when:

$$B_p B_\phi r^2 = \dot{M} \frac{\partial(v_\phi r)}{\partial r} \quad (4)$$

where B_p and B_ϕ are the poloidal and toroidal components of the NS magnetic field, r the radial coordinate measured from the NS center and v_ϕ the azimuthal velocity of the plasma at r . If one assumes that the transition region Δr connecting the unperturbed plasma flow far from the NS and the magnetospheric flow is much smaller than r_m , then the above equation takes the form:

$$B_p B_\phi r_m^2 \Delta r = \dot{M} v_\phi r_m \quad (5)$$

Once the gas reaches the transition region Δr , it stops flowing in Keplerian orbits and starts to co-rotate with the magnetosphere. The gas exchanges angular momentum with the magnetosphere and changes the NS spin frequency. The NS is spun up if its specific angular momentum is smaller than that of the accreting gas, and otherwise spun down. The spin-up/spin-down condition can be thought of in terms of characteristic radii: if r_m is smaller than the radius where the Keplerian frequency equals the NS spin frequency (the co-rotation radius r_{co}), the NS is spun up, otherwise it is spun down. The co-rotation radius can be defined as:

$$r_{co} = 1683 \left(\frac{M}{1.4 M_\odot} \right)^{1/3} v_s^{-2/3} \text{ km}. \quad (6)$$

It is important to stress that this is an over-simplified picture of the true physical conditions close in the inner disk. In this simple description, the accretion torque exerted on the NS for a Keplerian disk truncated at r_m , with $r_m < r_{co}$, is:

$$N = 2\pi I \dot{\nu}_s = \dot{M} \sqrt{GM r_m} \quad (7)$$

where I is the moment of inertia of the NS, $\dot{\nu}_s$ the NS spin frequency derivative and G the universal gravitational constant. At radii larger than the co-rotation radius, the magnetic field lines are threaded into the accretion disk and dragged by the high conductivity plasma so that an extra torque due to magnetic stresses has to be expected [227, 228, 232, 233] in addition to the torques due to the matter flow. Spin down due to dipole emission is also always present. A possible way to express the total torque acting on the pulsar is [234]:

$$N = \left(\dot{M} \sqrt{GM r_m} + \frac{\mu^2}{9r_m^3} \right) n(\omega) - \frac{\dot{E}_{dipole}}{2\pi \nu_s} \quad (8)$$

where \dot{E}_{dipole} is the energy loss due to dipole radiation and $n(\omega) \approx \pm 1$ is a dimensionless function that depends on the fastness parameter $\omega = (r_m/r_{co})^{3/2}$:

$$n(\omega) = \tanh\left(\frac{1-\omega}{\Delta r}\right) \quad (9)$$

This term takes account of the gradual transition from the spin-down to spin-up zone in the accretion disk [233, 234]. The two extra terms in Eq.(8) have a minor effect during most of the outburst, when the mass accretion has the largest weight in determining the net torque. The expression in Eq.(7) is therefore a good approximation most of the time.

As the AMXP is spun up, r_{co} moves towards and eventually reaches r_m . When this happens, the pulsar is said to have reached the ‘‘equilibrium spin period’’ P_{eq} :

$$P_{eq} \simeq 2.7 \left(\frac{B}{10^8 \text{ G}} \right)^{6/7} \left(\frac{M}{1.4 M_\odot} \right)^{-5/7} \left(\frac{\dot{M}}{10^{-10} M_\odot \text{ yr}^{-1}} \right)^{-3/7} \left(\frac{R}{10 \text{ km}} \right)^{18/7} \text{ ms} \quad (10)$$

Substituting into Eq.(10) the surface magnetic field (at the poles) derived from dipole spin down [235]:

$$B = \sqrt{\frac{6c^3 I P \dot{P}}{4\pi^2 R^6}} \frac{1}{\sin\alpha} \simeq 6.4 \times 10^{19} \text{ G} \sqrt{P \dot{P}} \left(\frac{M}{1.4 M_\odot} \right)^{3/2} \frac{1}{\sin\alpha} \quad (11)$$

(where we have assumed $I = 10^{45} \text{ g cm}^2$, $R = 10 \text{ km}$ and α is the misalignment angle between spin and magnetic axes), one obtains a relation between P_{eq} and \dot{P} . When the accretion rate reaches the maximum Eddington rate, this relation defines a ‘‘spin-up line’’ in the $P - \dot{P}$ diagram of radio pulsars (see Figure 5), above which millisecond radio pulsars should not be found. Indeed, if millisecond pulsars are created in LMXBs via accretion torques, then the maximum possible torque is set

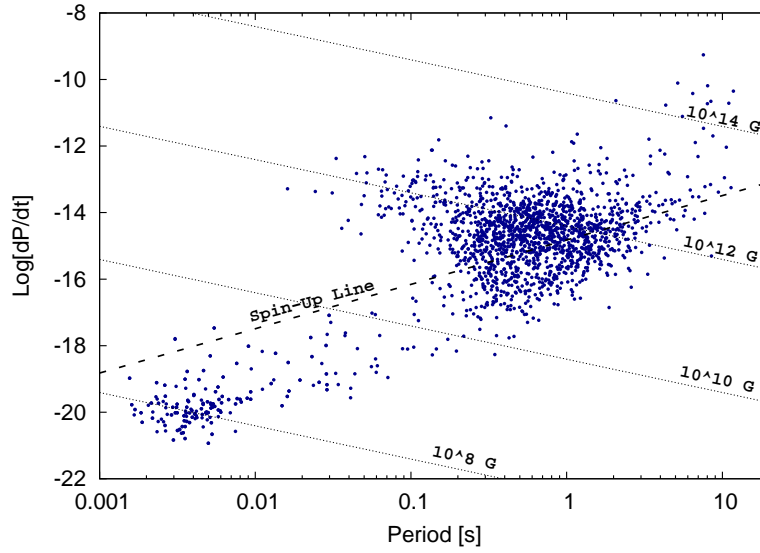


Fig. 5 $P - \dot{P}$ diagram of radio pulsars with a spin up line (dashed black line) above which radio pulsars should not be found if they are “recycled” via accretion. The black dotted lines identify magnetic fields of different strengths.

by the Eddington limit³ It is important to stress that the numerical solution of the force-free relativistic MHD equations lead to a similar (but slightly different) result for the dipolar magnetic field (again, at the poles) [237]:

$$B = \sqrt{\frac{c^3 I \dot{P}}{\pi^2 R^6}} \frac{1}{(1 + \sin^2 \alpha)^{1/2}} \simeq 5.2 \times 10^{19} \text{G} \sqrt{P \dot{P}} \left(\frac{M}{1.4 M_\odot} \right)^{3/2} \frac{1}{(1 + \sin^2 \alpha)^{1/2}} \quad (12)$$

To detect the effect of accretion torques in AMXPs one simply needs a measurement of \dot{v}_s , which in principle is straightforward when using coherent timing techniques. Unfortunately, however, determining the location of the magnetospheric radius is a non-trivial problem.

The main reason is that $\Delta r/r_m$ is assumed to be much smaller than unity, which is a good approximation only for slow accreting pulsars with high magnetic fields. This might not be the case for AMXPs with rapid rotation and weak magnetic fields (see for example Eq. 5 and the underlying assumptions).

³ Note, however, that the spin-up line depends on several parameters which are difficult to constrain like the angle α . Its position in the $P - \dot{P}$ diagram is therefore subject to uncertainties (see [236] for a discussion).

Furthermore we have considered so far only gas-pressure dominated accretion disks, considered to be a good assumption at the low average accretion rates of AMXPs. However, when the outbursts are close to their peak luminosities, radiation pressure may play a role in the exchange of angular momentum between the gas and the NS. At these accretion rates accreting plasma and magnetic field lines may couple and modify the amount of enhanced angular momentum [238, 239], thus invalidating the use of Eq.(7-8).

Noting these caveats, theoretical expectations for the average spin frequency derivative of an AMXP can be calculated with the simplest accretion model (Eq. 7) once one has a reasonable estimate of the mean mass accretion rate \dot{M} *during an outburst*. As discussed, such a measure is difficult to obtain, but several estimates of \dot{M} are present in the literature which can be taken as a first step to compare the measured $\dot{\nu}_s$ with the expected values (see for example [240] and [239]). The explicit expression for the expected $\dot{\nu}_s^{exp}$ can be obtained by substituting Eq.(2) into Eq.(7). The substitution gives:

$$\dot{\nu}_s^{exp} = 2.3 \times 10^{-14} \xi^{1/2} \dot{M}_{-10}^{6/7} M_{1.4}^{3/7} B_8^{2/7} R_{10}^{6/7} \text{ Hz s}^{-1} \quad (13)$$

where we have normalized all variables with their typical values as in Eq.(10).

As one can easily verify, the calculated values of $\dot{\nu}_s^{exp}$ are all of the order of $10^{-13} \text{ Hz s}^{-1}$ when neglecting the fact that at low mass accretion rates, when $r_m > r_{co}$ the ‘‘propeller regime’’ can set in, with the spin-down terms dominating in Eq.(8). In this phase, the specific angular momentum of the accreting plasma is insufficient for spin up to occur, and the centrifugal barrier removes angular momentum from the AMXP, slowing it down. It was originally suggested that centrifugal inhibition by the rotating magnetosphere would expel gas from the system and shut down the accretion process [241]. In fact for this to happen, r_m must exceed r_{co} by a margin of at least 1.3 so that matter can be accelerated to the escape velocity and can be flung out of the disk [87, 233, 88]. Accretion can in fact still take place, and two propeller regimes have been observed in 3D-MHD simulations of accreting pulsars [242, 243]: a ‘‘weak propeller’’ with no outflows and a ‘‘strong propeller’’ with expulsion of material. In both cases channeled accretion is still ongoing so that a spinning down AMXP could be in principle observed via coherent timing measurements in either propeller regime. The propeller is therefore expected to affect $\dot{\nu}_s$, but determining its onset is a very difficult task. Indeed, AMXP observations do not help much to constrain the theory in this case, since only weak evidence for possible propeller phases exists ([83, 184, 37, 217]). Coherent timing does not provide further insights, since the propeller is expected to start when the mass accretion (and thus the source luminosity) drops substantially, with a consequent decrease of the S/N of the pulsations. Furthermore the propeller may not last sufficiently long to allow measurement of the spin frequency derivative.

4.1 Coherent Timing Technique

Coherent timing analysis of the phase evolution of AMXPs can be performed after converting photon times of arrival from the spacecraft non-inertial reference frame to the Solar System barycenter (an approximate inertial reference frame) and correcting for general and special relativistic perturbations due to planets and minor bodies in the Solar System that affect photon propagation. Before discussing observational tests of accretion theory it is useful to clarify the observables that play a role in coherent timing studies. AMXPs show pulsations that are too weak to detect as single pulses: to reconstruct the signal it is necessary to fold the data in segments of several hundred seconds to obtain a pulse profile that is the average of several hundred thousand NS cycles. It is then possible to measure the fractional amplitude of the pulsations, and the pulse phase. Pulse profiles of AMXPs are generally highly sinusoidal, with little or no harmonic content beyond the fundamental frequency. In this case the pulse phases can be measured by choosing a fiducial point (e.g. the pulse peak) and tracking the variation of the phase at this point over time. Sometimes, however, strong harmonic content is observed, with the pulse profile shape varying during an outburst. This means that unlike in radio pulsar timing, where average profiles are often very stable, there is no stable fiducial point on which to base timing analysis. To avoid this problem it has become standard to decompose the pulse profile into its harmonic components and measure pulse amplitude b_k and phase ϕ_k of the k -th harmonic ($k = 1$ for the fundamental, $k = 2$ for the second harmonic and so on) via the expression:

$$x_j = b_0 + \sum_k b_k \cos \left[2\pi \left(\frac{k(j-0.5)}{N} - \phi_k \right) \right] \quad (14)$$

where b_0 is the unpulsed component, x_j is the number of counts detected in the j -th bin of the pulse profile, with $j = 1, 2, \dots, N$. This way the fiducial point of each harmonic is well defined since all harmonic components are pure sinusoids. The fractional amplitude can be measured by adding in quadrature the fractional amplitudes of each harmonic:

$$R = \left(\sum_k R_k^2 \right)^{1/2} = \sum_k \frac{N b_k}{N_{ph} - B} \quad (15)$$

where R_k is the fractional amplitude of the k -th harmonic, $N_{ph} = \sum_j x_j$ the total number of photons in a profile and B the total number of background photons. Note that this definition gives a fractional amplitude larger by a factor $\sqrt{2}$ than the often reported rms fractional amplitude. We use this definition of fractional amplitude since it has an immediate physical meaning as the pulsed flux fraction. To avoid confusion, we always refer to the fractional amplitude as ‘‘sinusoidal fractional amplitude’’ when we use the definition given in Eq.(15) or otherwise to ‘‘rms fractional amplitude’’. Note that in the AMXP literature ‘‘rms fractional amplitude’’, ‘‘sinusoidal fractional amplitude’’ and ‘‘peak-to-peak fractional amplitude’’ are also used.

This latter is calculated by measuring the flux at the peak and at the minimum of the pulse and dividing by the average flux.

Pulse phase can be measured as a function of time and each harmonic analyzed separately. We drop the subscript k from the phase symbols, since the following equations are valid for each harmonic. The pulse phase series can be decomposed into several terms encoding different physical effects:

$$\phi(t) = \phi_L + \phi_Q + \phi_{orb} + \phi_A + \phi_M + \phi_N \quad (16)$$

- $\phi_L = \phi_0 + vt$ is the linear term due to a *constant* spin of the NS (ϕ_0 is an initial reference phase)
- $\phi_Q = \frac{1}{2}\dot{v}t^2$ is the quadratic variation due to *constant* spin up or spin down
- ϕ_{orb} contains the effect of the orbital motion of the NS around the companion and, as a first order approximation, can be calculated by measuring the delays in the time of arrival of photons:

$$t_{em} = t_{arr} - \frac{A_1}{c} \sin i \sin \left[\frac{2\pi}{P_b} (t_{arr} - T_{asc}) \right] \quad (17)$$

where A_1 is the semi-major axis of the NS orbit, c the speed of light, i the inclination of the orbit with respect to the observer, T_{asc} the time of passage through the ascending node, P_b the orbital period and t_{em} and t_{arr} the photon emission and arrival time [244]. In this expression we have assumed that the orbit is perfectly circular, a good first order approximation in all AMXPs. More sophisticated models for nearly circular orbits can be found for example in [245].

- ϕ_A gives phase variations related to uncertainty in astrometric source position, which introduces a spurious frequency and frequency derivative offset. These offsets can be expressed as ([18]):

$$\Delta v = v_0 \varepsilon (a_{\oplus} \cos \beta / c) (2\pi / P_{\oplus}) \cos \tau \quad (18)$$

$$\Delta \dot{v} = -v_0 \varepsilon (a_{\oplus} \cos \beta / c) (2\pi / P_{\oplus})^2 \sin \tau \quad (19)$$

Here v_0 is the true pulse frequency, ε the position error parallel to the plane of the ecliptic, β the ecliptic latitude of the AMXP, a_{\oplus} and P_{\oplus} the Earth semi-major axis and orbital period and $\tau = 2\pi t / P_{\oplus}$ the orbital phase of the Earth. Phase zero is defined as the point where the Earth is closest to the AMXP and for order of magnitude estimates can be assumed such that $\cos \tau = \sin \tau = 1$.

- ϕ_M refers to unavoidable phase wandering due to measurement errors, and is normally distributed with an amplitude predictable by propagating the Poisson uncertainties due to counting statistics.
- ϕ_N is a subtle term covering residual phase variations that do not fall into any of the previous categories. These are usually called “X-ray timing noise”, by analogy with the timing noise often observed in radio pulsars. Note that if the spin-up (or spin-down) process is not constant in time we **do expect** terms higher than the quadratic (ϕ_Q) and these are considered, in our definition, as part of ϕ_N

even if they are true variations of the NS rotation. This should be expected if, for example, the accretion torques exhibit stochastic variations.

When performing coherent timing after having removed the ϕ_{orb} term and assuming that ϕ_A is negligible, the observer measures a pulse frequency and its time derivatives. These can be determined using a Taylor expansion:

$$\phi(t) = \phi_0 + \frac{\partial\phi}{\partial t}(t - t_0) + \frac{\partial^2\phi}{\partial t^2} \frac{(t - t_0)^2}{2!} + \dots \quad (20)$$

The parameters $\nu = \frac{\partial\phi}{\partial t}$, $\dot{\nu} = \frac{\partial^2\phi}{\partial t^2}$, etc., can be determined by fitting the pulse phases with standard χ^2 minimization techniques.

The *observable* quantities here are *not* the spin frequency ν_s and derivatives, but the pulse frequency ν and derivatives which are encoded as a combination of ϕ_L , ϕ_Q and ϕ_N . The pulse frequency is the frequency of the pulsations detected by the distant observer, whereas the spin frequency is the rotational rate of the NS as measured by the distant observer. The assumption that pulse and spin frequency (and derivatives) are identical may not always be true. For pulse and spin frequencies to be identical, ϕ_N must have no linear component. Similarly for the pulse and spin frequency derivative: only if ϕ_N has no quadratic component will the two be the same.

4.2 Observations: Accretion Torques in AMXPs

With the exception of the intermittent pulsar Aql X-1, all of the AMXPs have shown pulsations of sufficient quality and with a sufficiently long baseline to constrain the pulse frequency derivatives. As a rule of thumb, the condition that must be met to detect a pulse frequency derivative $\dot{\nu}$ in a data segment of length Δt is that $\sigma_{rms} < \dot{\nu}(\Delta t)^2$, where σ_{rms} is the root-mean-square error on pulse phases. Since all AMXPs (bar Aql X-1) have $\sigma_{rms} \sim 0.01$ cycles, and baselines of several days, we are sensitive to $\dot{\nu} \sim 10^{-15} - 10^{-13} \text{ Hz s}^{-1}$. These values overlap the range of expected $\dot{\nu}$ given by Eq.(7) for typical \dot{M} and weak dipolar B fields $\sim 10^8 - 10^9 \text{ G}$.

Several papers have reported pulse frequency derivatives in AMXPs. The first measure was made for the source IGR J00291+5934 [34] with a reported $\dot{\nu} = 8.4 \times 10^{-13} \text{ Hz s}^{-1}$ during its 2004 outburst. Table 3 summarizes the measurements for all AMXPs. However none of these values, including the measurement made for IGR J00291+5934, take into account the presence of X-ray timing noise in the pulse phases. One must therefore bear in mind that what is reported is the combined effect of ϕ_Q and ϕ_N , as explained in Section 4.1. Nevertheless timing noise has different strength in different sources, so that pulse and spin frequency derivatives may in some cases not be so dissimilar. We have marked each AMXP in Table 3 with a ‘‘w’’

for weak timing noise and “s” for strong. This distinction is somehow arbitrary, but is useful to understand the probability of the pulse frequency derivatives differing from the true spin frequency derivatives.

Table 3 Pulse Frequency and Spin Frequency Derivatives

Source	Pulse freq. deriv $\dot{\nu}$ (PFD) [Hz s ⁻¹]	Timing noise PFD strength	Reference	Spin freq. deriv $\dot{\nu}_s$ SFD (SFD) [Hz s ⁻¹]	SFD reference
SAX J1808.4-3658	4.4×10^{-13} ; -7.6×10^{-14}	s	[246]	$< 2.5 \times 10^{-14}$	[18, 19]
XTE J1807-294	2.5×10^{-14}	s	[29]	$< 4 \times 10^{-14}$	[247]
IGR J00291+5934	$[5; 11] \times 10^{-13}$	w	[34, 35, 38]	$+5.5 \times 10^{-13}$	[34, 35, 36, 37, 38]
XTE J1814-338	-6.7×10^{-14}	s	[32]	$< 1.5 \times 10^{-14}$	[248]
XTE J0929-314	$-9.2(4) \times 10^{-14}$	s	[25]		
XTE J1751-305	5.6×10^{-13}	w	[23]		
IGR J17511-3057	1.6×10^{-13}	s	[48]		
IGR J17498-2921	-6.3×10^{-14}	w	[50]		
HETE J1900.1-2455		s		$[2.3; 0.4] \times 10^{-13}$	[64]
Swift J1756.9-2508		w		$< 3 \times 10^{-13}$	[41]
Swift J1749.4-2807		s		$< 1.2 \times 10^{-12}$	[204]
IGR J18245-2452		?		$< 1.3 \times 10^{-12}$	[12]

The AMXPs Aql X-1, SAX J1748.9-2021 and NGC 6440 X-2 do not appear in the table above as the observing baseline is too short to provide meaningful upper limits.

To verify whether the pulse frequency derivative is a robust indicator of the spin frequency derivative $\dot{\nu}_s$, one has to investigate the strength of ϕ_N on the timescales over which $\dot{\nu}$ is measured. To do this, one can use Monte Carlo (MC) simulations to estimate the true uncertainty on the pulse frequency derivative [18]. The MC method works as follows: one fits a second-order polynomial to measure ν and $\dot{\nu}$ with standard χ^2 minimization techniques after having removed all other effects (such as orbital variations) and obtains an estimate of $\nu \pm \sigma_\nu$ and $\dot{\nu} \pm \sigma_{\dot{\nu}}$. If in the phase residuals there are still substantial variations of the pulse phase, in excess of that expected from measurement errors alone (i.e., ϕ_M) - which can be verified by checking whether χ^2 gives a statistically unacceptable fit - then the statistical errors σ_ν and $\sigma_{\dot{\nu}}$ are not good representations of the true uncertainties of the spin parameters. Instead one can take the phase residuals, calculate a power spectrum and simulate several thousand time series with nearly identical noise content as the original phase residual time series [18]. At this point ν and $\dot{\nu}$ can be measured for each simulated time series, and a distribution of parameters constructed. The standard deviation of the distribution of ν and $\dot{\nu}$ provides a good representation of the true uncertainties on the spin parameters. In this way one can immediately check whether the noise content ϕ_N affects the measured value of ν and $\dot{\nu}$. Applying this technique has revealed discrepancies between pulse and spin parameters in several AMXPs (Table 3). The most striking finding has been the non-detection of spin frequency derivatives in several AMXPs, with upper limits below the expected $\dot{\nu}_s$.

The use of MC simulations is not the final word on this problem, since the origin of timing noise remains unexplained. It also has its limitations: if the lowest Fourier frequency component of timing noise is comparable to the length of the data segment over which ν and $\dot{\nu}$ are measured, MC simulations cannot distinguish pulse

and spin parameters. It has been noted that the phase residuals obtained after removing ν and $\dot{\nu}$ from the pulse phases of two AMXPs (XTE J1814-338 and XTE 1807-294) are anti-correlated with variations in X-ray flux [32, 29]. The anti-correlation improves substantially if one fits a simple $\nu = \text{const}$ model, suggesting that timing noise, which is related to the X-ray flux variations, is almost entirely responsible for the measured $\dot{\nu}$ [249]. Correlations (or anti-correlations) between pulse phase residuals (with respect to a $\nu = \text{const}$ model) and X-ray flux have now been found in at least six AMXPs where such studies have been carried out [249]. In some cases the correlation was striking (e.g., in XTE J1814-338 [248]) leaving little doubt that the pulse frequency derivative $\dot{\nu}$ is **not** the spin frequency derivative $\dot{\nu}_s$. This discovery also suggests that **it is the pulse phase ϕ and not its second derivative ($\dot{\nu}$) that correlates with the flux** (and thus the mass accretion rate), as would instead be expected from Eq.(7). One way to test these findings is to measure “instantaneous” short timescale spin frequencies and check whether these scale with the bolometric flux as $\dot{\nu}_s \propto F_{bol}^\gamma$, where γ is a scale factor that depends on accretion disk structure. The bolometric flux is, however, almost never available, since observations usually cover only a narrow (high) energy band. If we assume that the X-ray flux is $F_X \propto F_{bol}$ then we expect to see $\dot{\nu}_s \propto F_X^\gamma$. However this assumes that the mass accretion rate $\dot{M} \propto F_X$, which has been shown to be untrue in some LMXBs [250]. There is one additional complication: AMXPs have outbursts that are almost always too short to split data segments long enough to yield more than one short-term “instantaneous” spin frequency derivative.

If one keeps these caveats in mind, then it is possible to test the relation between $\dot{\nu}_s$ and F_X for some AMXPs, such as XTE J1807-294 and XTE J1814-338 which have shown long outbursts (~ 100 and ~ 40 days, respectively) and high S/N ratio for the pulsations. In XTE J1807-294, the “instantaneous” $\dot{\nu}$ changes sign several times during the outburst decay and all “instantaneous” spin frequency derivatives $\dot{\nu}_s$ are insignificant and consistent with being part of the underlying timing noise process [247]. In XTE J1814-338, the instantaneous $\dot{\nu}$ are too large (up to $10^{-11} \text{ Hz s}^{-1}$) to be physically meaningful, requiring accretion rates well above the Eddington limit [251]. This is at odds with the fact that AMXPs are faint and rarely reach accretion rates above 10% Eddington, suggesting that $\dot{\nu}$ is different to $\dot{\nu}_s$ and is completely dominated by timing noise. This does not prove that $\dot{\nu}_s$ does not scale with flux, but only that measurements of “instantaneous” $\dot{\nu}_s$ are contaminated by timing noise, which prevents testing of the relation between $\dot{\nu}_s$ and F_X .

Theoretical expectations for $\dot{\nu}_s$ mostly exceed observed values measured by taking into account the contamination of timing noise (Table 3). This means that most AMXPs do not behave in accordance with the predictions of accretion torque theory (Eq.8). In addition, once gas attaches to the magnetic field lines of the AMXP, an exchange of angular momentum is inevitable unless $r_m = r_{co}$. But this cannot be the case throughout an outburst: $r_m \propto \dot{M}^{-2/7}$ and the mass accretion rate varies, so r_m must at some point differ from r_{co} . Larger torques, which are expected close to the outburst peak, are clearly ruled out in some AMXPs [18, 30, 248]. The angular momentum of the accreting plasma must however be transferred somewhere so that the mismatch between expected and observed $\dot{\nu}_s$ appears problematic.

4.2.1 The Origin of X-ray Timing Noise

The phase wandering of pulsations in coherent timing analysis requires careful consideration if we are to understand how a NS responds to accretion. Theoretically the phenomenon is easy to explain if one assumes that the accretion hot spot is not completely anchored to one location on the surface. One possibility is that the magnetic and rotational axes of the NS are almost aligned and the hot spot wanders around the magnetic axis by small displacements, generating large variations in phase and amplitude [253]. In this case pulsed fractions and times of arrivals should be anti-correlated. A moving hot spot has been observed in 3D-MHD simulations of magnetized accreting NSs [254, 252]. In particular, it was shown that the usual assumption of a fixed hot spot is valid only for large misalignment angles between the magnetic and spin axes (Figure 6, [252]), in good agreement with the magnetic and rotational axis alignment model [255, 253]. This strengthens the idea that most X-ray timing noise may be related to a moving hot spot configuration. Alternatively, the phase wandering might be related to complexity in the structure of the pulsar's magnetic field, with different multipole components dominating the accretion process at different accretion rates [256].

Timing noise may also be due to fluctuating accretion torques [257, 258]. This has been studied for strongly magnetized accreting pulsars like Vela X-1 [259], and it is natural to expect something similar in AMXPs. However as discussed,

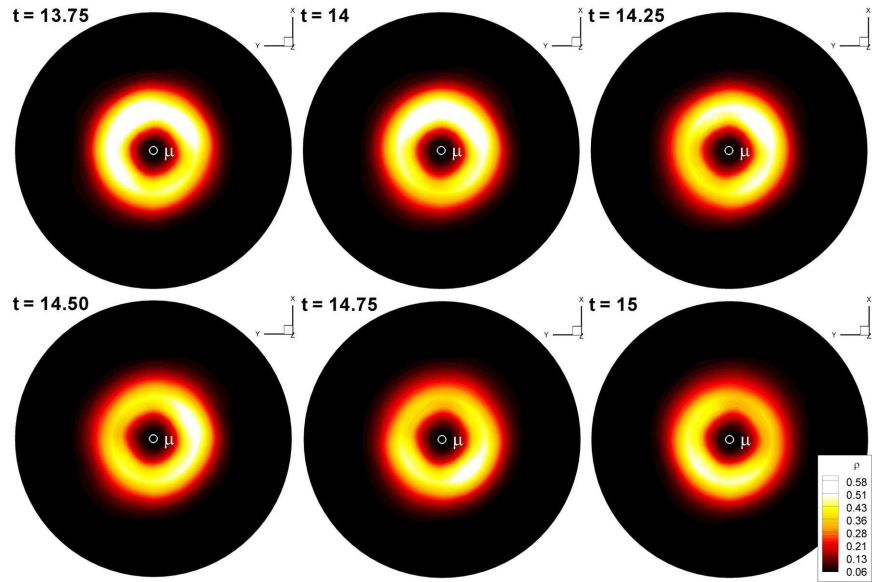


Fig. 6 Evolution of the position of the hot spot during accretion ($v_s = 4.1$ ms). μ represents the magnetic dipole axis. Note how the densest portion of the circular hot spot (encoded by the ρ scale, bottom right) shifts during time even if the observer is in the rotating reference frame of the NS (Figure from [252].)

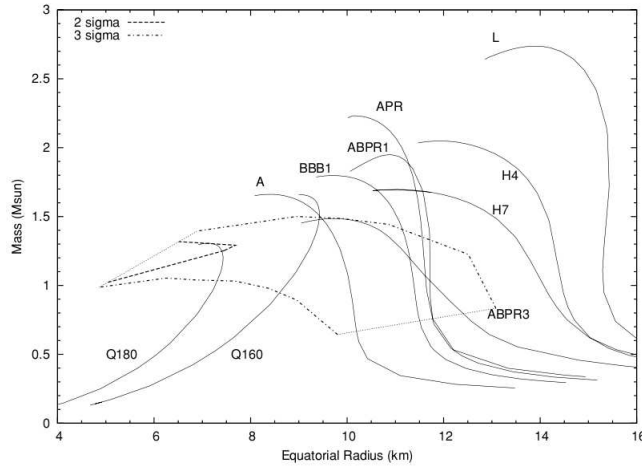


Fig. 7 Mass-Radius relation for several different EoS of ultra-dense matter, and constraints on the M-R relation of the AMXP SAX J1808.4–3658. These result from modeling pulse profiles observed in the 1998 and 2002 outbursts (Figure from [264]).

this model requires unphysical large accretion rate fluctuations to explain all timing noise or the large jumps in phase observed for example in XTE J1814–338 (and probably also SAX J1808.4–3658 and XTE J1807–294, [32, 29, 249, 251, 18]). Nonetheless some X-ray timing noise, or even its entirety for AMXPs with weak timing noise content, could in principle be related to accretion torque fluctuations.

5 Pulse Profiles

AMXP pulse profiles form in regions of strong gravity and encode information about the physical properties of the emitting regions and the compactness of the NS [260, 261, 262, 263, 264]. Light bending, aberration and relativistic Doppler shifts all affect pulse profile shape [265, 266, 267, 268] and can be measured using coherent timing analysis. This can be used to constrain the EoS of ultra-dense matter (Figure 7) although large uncertainties still exist: in part due to model-dependencies, but more importantly because of the low S/N of the relativistic features.

Pulse profile shapes can also constrain the geometry of the NS magnetic field [269, 270, 271] since multipoles generate different accretion columns and hot spots on the NS surface (see, however, [272], for a recent discussion of the problem). The information contained in pulse profiles can be extracted by studying pulse amplitudes, the harmonic content of the signal and the time of arrival of the pulsations. Double peaked pulse profiles, for example, may be observed when two antipodal hot-spots exist on the NS surface [266, 253, 268]; a high harmonic content is suggestive of a complex field geometry [273] and the energy dependence of the pulse am-

plitudes and the time lags of the pulsations provide a way to explore the angular pattern of the radiation emitted from the NS surface [260, 117, 268]. The temporal evolution of the pulse shapes also reveals details of the complex disk/magnetospheric interaction responsible for magnetic channeling of the accreting plasma [274, 94].

5.1 Pulse Fractional Amplitudes and Phase Lags

The pulse profiles of AMXPs are sinusoidal, with only the fundamental frequency detected in most cases (including IGR J00291+5934, XTE J0929–314, XTE J1751–305, SAX J1748.9–2021 and IGR J17498–2921). In some AMXPs there is a first overtone (e.g. XTE J1814–338, IGR J18245–2452 and NGC 6440 X-2), and higher overtones are seen only sporadically in just three AMXPs (SAX J1808.4–3648, Swift J1749.4–2807 and XTE J1807–294). Pulse fractional amplitudes reach values of a few percent, with the highest sinusoidal amplitude measured being 30–40% (Swift J1749.4–2807 and XTE J1807–294) and the lowest being 0.3% (HETE J1900.1–2455). With the exception of Swift J1749.4–2807, overtones do not generally contribute to the amplitude of the pulsations by more than about $\sim 5\%$.

All AMXPs show an energy dependence of the pulse fractional amplitudes. In some sources the fractional amplitude increases steeply with energy, e.g. Aql X-1 [42] Swift J1756.9–2508 [30] and SAX J1748.9–2021 [44]. In this latter source, the fractional amplitude increases by a factor ~ 10 between 2 and ~ 20 keV. Some AMXPs have fractional amplitudes that drop with energy (SAX J1808.4–3658 [275], XTE J1751–305 [117], XTE J0929–314 [63], HETE J1900.1–2455 [63], IGR J17511–3057 [94, 191]). Other AMXPs (IGR J00291+5934 and XTE J1807–294) are more complex, with the amplitude rising and falling in different energy bands [34, 30]. The energy dependence of the pulsed fractions provides insights into the pulse formation process, since a simple hot spot emitting blackbody radiation with a temperature contrast with respect to the NS surface would produce pulsations which increase in amplitude at higher energies in the observer reference frame [266].

Another interesting finding has been the correlation or anti-correlation between the fractional amplitude of the fundamental (where most of the pulse power is observed) and the time of arrival of the pulsations of some AMXPs. The most prominent example is XTE J1807–294 where high/low fractional amplitude pulses arrive systematically earlier/later than predicted by the timing model. This finding, and a similar anti-correlation between the time of arrivals and the X-ray flux, may be evidence for a hot spot moving on the NS surface [30]. Similar conclusions were reached by other authors to explain the timing noise observed in the timing residuals of several AMXPs [44, 18, 29, 32]. Some of these observations can be understood in terms of the hot spot wandering model described in Section 4.2.1 although no final confirmation of the models has yet been put forward. Despite many open problems that need to be solved (such as why such correlations are not observed in

AMXPs like SAX J1808.4–3658) the moving hot spot model help us to understand the AMXP pulse formation process.

Soon after the first AMXP discovery, it was realized that the lowest energy (“soft”) photons that compose the pulsations arrive on average later than the high energy (“hard”) photons [275]. In SAX J1808.4–3658, hard photon arrival times tend to saturate at some energy $E \gtrsim 10$ keV, with soft photons at about 2 keV accumulating a lag of about 0.08 rotational cycles (or 200 μ s). Similar behaviour was soon discovered in other five AMXPs: XTE J0929–314 (0.14 cycles [25]), XTE J1751–305 (0.06 cycles, [117]), XTE J1814–338 (0.016 cycles, [276]), XTE J1807–294 (0.1 cycles, [28]) and in the intermittent pulsar HETE J1900.1–2455 (0.07 cycles, [63]). In IGR J00291+5934, soft lags were observed with hard photons leading by 0.06 cycles at 6–8 keV [34]. Above this energy, harder photons ($E \gtrsim 8$ keV) start to gradually reduce their lead until at energies of 30–100 keV there are no phase lags with respect to the soft photons (at ~ 2 keV). The origin of these lags is poorly understood, and has been discussed in terms of the different angular distribution (“fan” and “pencil” beams) of a two spectral component model [260] or in terms of Compton down-scattering of hard X-ray photons from the cold disk plasma or the NS surface [151]. Detailed study of the soft lags in SAX J1808.4–3658 [277] suggests that they have a flux dependence, with the lag being almost zero at high fluxes, increasing steadily at lower fluxes and then decreasing again below a flux threshold coincident with the onset of the rapid decay. This may be linked with the changing properties of the accretion disk as it transitions towards the propeller phase.

5.2 Pulse Shape Evolution

Most AMXPs with strong harmonic content show pulse shape variability that often correlates with the stage of the outburst. The pulse profiles observed in *different* outbursts of SAX J1808.4–3658 have characteristic shapes that can be associated with the specific stage of the outburst (e.g., rise, peak, decay, etc.; see [18, 94, 278]). There is a very strong linear anti-correlation between the fractional amplitude of the first overtone and the X-ray flux (something very similar was also observed in XTE J1807–294; [30]), suggesting that the secondary hot spot becomes visible or more prominent as the accretion process becomes less intense. This may be explained if the inner disk radius moves in or out with respect to the accretion rate, rendering the secondary hot-spot visible [18, 94]. If the inner disk radius r_{in} is assumed to vary at different outburst stages, then the pulse profile changes of SAX J1808.4–3658 can be explained in this way [279]. Variations in the disk-magnetosphere coupling may also explain explain some of the pulse shape and phase variations [278]. Calculation of the light-curve of accreting NSs in global 3D-MHD simulations showed that if an octupolar magnetic field dominates the field configuration, double peaked pulse profiles can be reproduced [256]. Similar pulse shape variations were seen to correlate with the outburst stage of Swift J1756.9–2508 [30] IGR J17511–3057 [94] and to some extent XTE J1807–294 [36]. However, to date it is still unclear why pulse

profiles change abruptly and unpredictably in some sources during certain outbursts but at other times have limited variability.

6 Long Term Evolution and Pulse Formation Process

If AMXP pulsations are observed in different outbursts one can follow the long-term spin and orbital evolution. To date only five AMXPs have been monitored with high time resolution instruments in different outbursts: SAX J1808.4–3658, IGR J00291+5934, XTE J1751–305, Swift J1756.9–2508 and NGC6440 X-2 (although with relatively low S/N and short outburst duration, it is difficult to constrain the long-term evolution of the latter two).

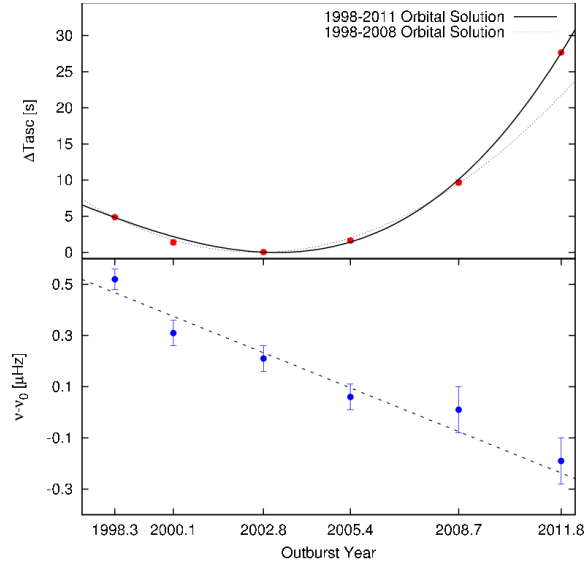
6.1 Specific sources

SAX J1808.4–3658 The best constrained AMXP is SAX J1808.4–3658, for which secular spin evolution and orbital period variation have now been measured over a 13 year baseline [17, 18, 19]. As discussed previously, accretion torques have a small effect on the spin of SAX J1808.4–3658 and have never been conclusively detected during any of the six outbursts monitored by *RXTE*. However, if one compares the constant spin frequency measured in each outburst, SAX J1808.4–3658 is clearly spinning down at a constant rate (bottom panel in Figure 8; [17]). The stability of the spin-down rate suggests that its origin is unrelated to propeller onset, since spin-down would then depend on the amount of mass propelled and on the duration of this phase, which can vary from outburst to outburst. Loss of angular momentum via emission of gravitational waves was also considered [18], and is interesting since this might also balance accretion torques, explaining the lack of measurable spin-up during the outbursts. However, fine tuning is also required in this case since the mechanism producing gravitational waves has to be triggered for the right amount of time so as to guarantee a constant spin-down between outbursts [17, 248, 19]. The most likely scenario appears to be a loss of angular momentum via magnetic-dipole radiation. This is expected for any rapidly rotating NS with a magnetic field, even if the NS does not turn on as a radio pulsar. The measured spin-down is of the order of $-10^{15} \text{ Hz s}^{-1}$ and is consistent with a polar magnetic field of $2 \times 10^8 \text{ G}$ [17, 18, 19].

The long-term orbital evolution of SAX J1808.4–3658 is also exciting. Theory states this should be driven by loss of angular momentum via emission of gravitational waves from the tight binary orbit. For SAX J1808.4–3658, the resulting orbital evolution should proceed on a timescale $\sim 10^9$ years [280]:

$$\tau_{\text{GW}} = 0.01 \frac{(M_{\text{NS}} + M_2)^{1/3}}{M_{\text{NS}} M_2} P_b^{8/3} \text{ Gyr} \quad (21)$$

Fig. 8 Orbital (top panel) and spin frequency evolution (bottom panel) of SAX J1808.4–3658 over a baseline of 13 years. The top panel shows the delays accumulated by the pulsar as it passes through the ascending node. The data were consistent until 2008 with a parabolic increase which is equivalent to a steady widening of the orbit (dotted line). The 2011 data revealed instead an acceleration of the orbit, as evidenced by the solid line in the top panel. The spin frequency has shown a steady decrease in between outbursts (bottom panel; ν_0 is a frequency offset of 400.975210 Hz), compatible with a spin down of the order of $-10^{-15} \text{ Hz s}^{-1}$. (Figure from [17]).



where P_b is in hours and M_{NS} and M_2 are the NS and donor masses. The observed value, however, implies an expansion of the orbit on a timescale of ~ 70 Myr [18, 19, 281, 282]. Further observations in 2011 provided a long enough baseline to detect an orbital period acceleration (top panel in Figure 8; [17]). SAX J1808.4–3658 may therefore behave like the “black widow” binary millisecond pulsars observed at radio frequencies [283] with a short-term exchange of angular momentum between the donor star and the orbit. A similar suggestion was also previously proposed for this AMXP [282, 281], invoking a “hidden” black widow scenario in which the AMXP switches on as a radio pulsar during quiescence and ablates its donor.

IGR J00291+5934 Long-term spin down has also been measured between the 2004 and 2008 outbursts of IGR J00291+5934. The AMXP rotation behaves like a saw-tooth, spinning up during the 2004 outburst then spinning down until the 2008 outburst. The spin-down rate is $\approx -3 \times 10^{-15} \text{ Hz s}^{-1}$ [30, 37, 38], comparable to that observed in SAX J1808.4–3658. Although spin down between outbursts has been observed only once and it is not possible (until the next outburst) to verify whether it is constant, the most likely explanation also involves magnetic dipole radiation spin-down. If this saw-tooth behaviour is a good indicator of the *secular* spin evolution of this AMXP, then the net spin frequency is *increasing* at $\approx +2.5 \times 10^{-15} \text{ Hz s}^{-1}$. Indeed, the spin frequency at the beginning of the 2004 outburst was less than that observed in the 2008 outburst: the 2004 spin-up accelerated the pulsar more than it subsequently decelerated in quiescence. The relatively small baseline did not permit

any useful constraints on orbital period evolution: this should be possible after the observation of the next outburst.

XTE J1751–305 Comparing the spin frequencies from 2002, 2005, 2007 and 2009 reveals a secular spin down of $-5.5 \times 10^{-15} \text{ Hz s}^{-1}$ [284]. This is again consistent with magnetic dipole spin-down. If the spin-up measured during the 2005 outburst reported in [23] is not strongly affected by timing noise, then its behaviour resembles IGR J00291+5934, with spin frequency increasing in outburst and decreasing between outbursts in a saw-tooth. The inferred magnetic field is $\sim 4 \times 10^8 \text{ G}$, in line with the other two AMXPs constrained in this way. The low quality of the data taken in the 2002 outburst does not permit stringent constraints on orbital evolution.

Swift J1756.9-2508 Observations during the outbursts in 2007 and 2009 give upper limits of $|\dot{\nu}| \lesssim 2 \times 10^{-15} \text{ Hz s}^{-1}$ on the secular spin evolution of this AMXP [30]. This requires a magnetic field $< 9 \times 10^8 \text{ G}$. Magnetic field estimates for all four of these AMXPs are given in Table 6.1.

Source	Spin-Down in Quiescence [Hz s ⁻¹]	Magnetic Field [10 ⁸ G]	Secular Evolution	Reference
SAX J1808.4-3658	-10^{-15}	1.5-2.5	Spin-down	[17, 18, 19]
IGR J00291+5934	-3×10^{-15}	1.5-2.0	Spin-up	[30, 37, 38]
XTE J1751–305	-5.5×10^{-15}	4	Spin-down	[284]
Swift J1756.9-2508	$< 2 \times 10^{-15}$	< 9	?	[44]

Table 4 Secular Evolution and Inferred Magnetic Fields in AMXPs. The magnetic field is inferred from the spin down observed in quiescence, and refers to field at the poles of the NS for a pure dipolar configuration, $R = 10 \text{ km}$ and $M = 1.4 M_{\odot}$.

6.2 The Maximum Spin Frequency of Neutron Stars

None of the AMXPs discussed above has a spin rate that *increases* on long timescales, except for IGR J00291+5934. Even this source has a *net* acceleration so small that its spin frequency will change significantly only on timescales of several billion years. This raises the question on whether this behavior is the norm for AMXPs.

For all realistic EoS of ultra-dense matter, NSs are stable at spin frequencies well in excess of 1000 Hz. The break-up frequency is well approximated by

$$v_{\text{max}} = 1230 \left(\frac{M_{\text{NS}}}{1.4 M_{\odot}} \right)^{1/2} \left(\frac{R_{\text{NS}}}{10 \text{ km}} \right)^{-3/2} \text{ Hz} \quad (22)$$

(where M_{NS} and R_{NS} refer to the non-rotating mass and radius of the NS under consideration, expression valid for arbitrary NS mass and EoS as long as the mass is not too close to the maximum permitted for that EoS [285, 286]). However the distribution of spin frequencies of the ensemble of AMXPs and NXPs (nuclear powered

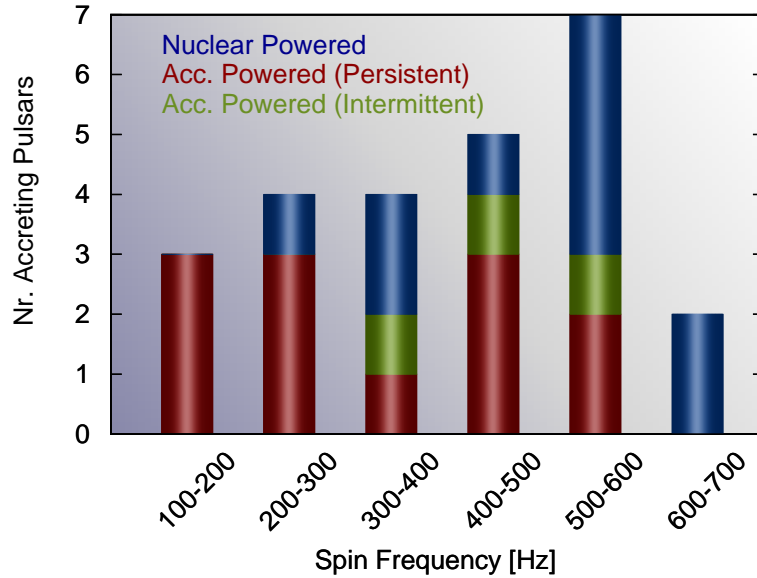


Fig. 9 Histogram of the spin frequency of AMXPs (both intermittent and persistent pulsators) and NXPs. The histogram is empty for frequencies larger than about 700 Hz. This is similar to what is found in radio pulsar data, where the sample size is considerably larger (with hundreds of millisecond radio pulsars).

X-ray pulsars, see Introduction and Section 7) has an abrupt cutoff at about 730 Hz. This was first noticed in 2003 [95] and has been confirmed in later works with larger sample size [287, 36]. Figure 9 shows the current distribution of spin frequencies for the 15 AMXPs and the 10 NXPs known (see Table 1 in [288] for a complete list of NXPs). So far no AMXP or radio millisecond pulsar has been found above this cutoff (the fastest radio millisecond pulsar has a spin of 716 Hz [289]). So not only there are no pulsars with $\nu_s \gtrsim 700$ Hz, but also at least four AMXPs that should be accelerating in response to accretion are instead either decelerating or spinning up very slowly, on timescales of billions of years.

Gravitational waves have been invoked to explain this cutoff, but as shown recently [37, 38, 248], this cannot be the explanation for all AMXPs as it would require substantial fine-tuning to explain the X-ray timing observations. The cut-off might instead be related to the magnetic field evolution of NSs [239]. However, further investigation is needed to assess this fascinating question in a robust way since it is still unclear how the magnetic field of NSs evolves in response to accretion [290, 291, 292, 293, 294, 295].

6.3 Why do most Low Mass X-ray Binaries not pulsate?

Even after 15 years of high time resolution X-ray observations, only a few LMXBs have shown millisecond pulsations. Several LMXBs have pulsations at long periods (Table 1) but the number of pulsating systems is still small compared to the entire LMXB population. Several mechanisms have been proposed to solve this problem, including burial of the magnetic field by accretion [296, 290, 297], smearing of the pulsations by an optically thick corona [298, 299, 300], smearing of pulsations due to gravitational light bending [301, 302], alignment of the NS magnetic and rotational axes [255, 253] and onset of MHD instabilities at the disk/magnetospheric boundary [303]. None of these models have yet been confirmed, although several new findings have helped to test their predictions.

Magnetic Field Screening. In this model, fresh unmagnetized accreted plasma diamagnetically screens the NS magnetic field as it is deposited on the surface [296, 290, 297]. The field then re-emerges via Ohmic diffusion and competition between the Ohmic diffusion and accretion timescale sets the behaviour of the magnetic field. If the accretion timescale is shorter than the Ohmic diffusion timescale, the magnetic field is buried deep in the ocean and outer crust. The two timescales can be defined as:

$$\tau_{\text{acc}} = \frac{y}{\dot{m}} \quad (23)$$

$$\tau_{\text{diff}} = \frac{H^2}{\eta} \quad (24)$$

where $y = \rho dz$ is the column density, z is the direction orthogonal to the surface in the plane parallel geometry approximation, \dot{m} is the local mass accretion rate per unit area (in units of $\text{g cm}^{-2} \text{s}^{-1}$), $H = \frac{d \ln P}{dz}$ is the pressure (defined as P) scale-height, and η is the magnetic diffusivity coefficient. This model predicts that LMXBs with very low mass accretion rates should be AMXPs, and that the most luminous LMXBs should not pulsate. This seems to be the case, since persistently pulsating AMXPs are indeed all faint LMXBs. However, the discovery of intermittent pulsations as short as ~ 100 seconds in Aql X-1 poses severe problems for the model since it is unclear how a buried B field could emerge for this brief episode. Another interesting observational result comes from HETE J1900.1–2455, which, with a mean bolometric luminosity of $4.4 \times 10^{36} \text{ erg s}^{-1}$, has a mean mass accretion rate $\dot{M} \approx 8 \times 10^{-10} M_{\odot} \text{ yr}^{-1}$ for an assumed accretion efficiency of 20%. This accretion rate is about twice that of most AMXPs, but is smaller than the bolometric luminosity of SAX J1808.4–3658 during observations taken close to the peak of the 2008 outburst [278]. This might indicate that the screening timescale is long compared to the outburst duration of most AMXPs. In HETE J1900.1–2455 observational evidence for magnetic field screening has been found [64], with the magnetic field possibly reducing by orders of magnitude on a timescale of about 100 days during which channeled accretion becomes less and less efficient until it stops working. If confirmed this indicates that indeed most LMXBs might be not pulsating

because of the lack of an extended magnetosphere. Recent 2-D and 3-D numerical simulations have started to address this problem and results seem to suggest that submergence of the magnetic field is possible at least when the accretion rate is high ([304] but see also [305, 306, 307] for different results). Despite still open problems, the screening model remains therefore one of the most promising, although further efforts are necessary to formulate new sophisticated predictions and tests.

Smearing from an Optically Thick Corona. This model suggests that X-ray emission from AMXPs is formed primarily via Comptonization processes in a relatively optically thin medium. If the Compton cloud is thick, then pulsations can be washed out. This scenario has been criticized on the grounds that spectral analyses of most LMXBs show small optical depths, well below the limit required to smear out pulsations [308], which should therefore be visible (but see [300]). It is not clear why in this model the intermittent AMXP SAX J1748.9–2021 shows pulsations that appear and disappear on timescales of a few hundred seconds [45, 44], uncorrelated with spectral changes. However it provides a reasonable explanation for the time lags and pulse energy dependence, especially for the pulses of IGR J00291+5934 which have a turnover at 7 keV that is otherwise difficult to explain [34, 151].

Gravitational Light Bending. For large stellar compactness (M/R), gravitational light bending can distort the path of X-ray photons up to the point where pulsations are strongly reduced [302, 309, 301]. Persistent sources may therefore be less likely to show pulsations because they accrete more mass than transient systems. However, the total amount of mass that a NS has accreted does not depend on the current mass accretion rate and on the persistence of the X-ray flux, but on the evolutionary stage of the donor star and on the average mass transfer rate from the donor towards the accretor. This model also requires that the NSs in most LMXBs are more massive than those in AMXPs. Although possible, this is difficult to reconcile with the fact that most AMXPs have probably accreted for a long time (see for example [14]). The model also requires some special configuration of the accretion column, which existed for only a very short time and has never recurred, to explain the short pulsed episode of Aql X-1. Finally, the light bending effect never suppresses completely oscillation amplitudes since the Doppler shift due to the rapid NS rotation introduces anisotropies in the emission pattern and thus pulsations [310, 268].

Magnetic and Rotational Axes alignment. The possibility that the magnetic poles of NS migrate was first suggested by Ruderman in 1991 [255]. Vortex/fluxoid coupling in the NS interior links the spin and magnetic axes. Once the NS is spun-up by accretion, crustal shear stress breaks the crust into “plates” that drift towards the rotational poles. The phenomenology of an AMXP with a nearly aligned magnetic and rotational axis was developed recently [253] and explains fairly well the observed correlations between pulse amplitude, pulse phase and X-ray flux. The model can explain intermittency [311], but implies that the persistent AMXPs should also show occasional “oscillation dropouts”, a sudden and brief disappearance of pulsations due to sporadic alignment of the hot spot and rotational axis. Such dropouts have not been observed, although the timescale over which this might happen may be too

short compared to timescale over which the pulsations are measured (i.e., hundreds of seconds). The model also predicts correlations between excess background noise produced by the hot spot motion which is anti-correlated with the pulse amplitude. This prediction could in principle be easily verified in the future with observational tests.

MHD Instabilities. Accretion onto a magnetized NS can proceed via channeled accretion but also via the Schwarzschild-Kruskal instability (the magnetic version of the Rayleigh-Taylor instability) in the disk equatorial plane ([312, 313]). This latter mode of accretion has now been observed in 3D-MHD simulations ([314]) and predicts a decoherence of the X-ray signal at high accretion rates, when several “tongues” of plasma penetrate the magnetosphere and impact the NS surface at random positions. This model explains why bright LMXBs do not pulsate, and might explain why intermittent sources are on average brighter than persistent AMXPs. However, the intermittent AMXP SAX J1748.9–2021 has shown pulsations that appear and disappear in a broad range of accretion rates [44] (rather than at a sharp threshold). It is also hard to explain why tongues never develop in any other AMXP when the outbursts reach peak luminosity, during which the accretion rates are comparable or higher than observed in intermittent AMXPs.

7 Thermonuclear Bursts

Source	Burst osc. Phase locking		References
Accreting Millisecond X-Ray Pulsars			
SAX J1808.4–3658	Yes	No	[77, 78, 95, 315, 85, 316, 317]
XTE J1814–338	Yes	Yes	[318, 319, 320, 321, 251, 317]
Aql X–1	Yes	No	[322, 323, 324, 166, 325, 326, 317]
SAX J1748.9–2021	No		[175, 327, 45, 317]
HETE J1900.1–2455	Yes	No	[328, 150, 63, 317, 329]
IGR J17511–3057	Yes	No	[187, 188, 330, 48]
IGR J17498–2921	Yes	Unknown	[208, 209]
Swift J1749.4–2807	No		[196, 205]
IGR J18245–2452	Yes	Possible	[222, 12, 331]
Mildly Recycled X-ray Pulsar			
IGR J17480–2466	Yes	Yes	[53, 332, 333, 334, 335, 336]

Table 5 Burst oscillation properties for the nine AMXPs that have shown thermonuclear bursts. The table indicates whether a source shows burst oscillations and whether their phases match and follow the evolution of the accretion-powered pulses observed before and after the bursts (“Phase Locking”).

Type I X-ray bursts are thermonuclear explosions triggered by unstable burning of hydrogen or helium on the layers that build up on the surfaces of accreting NSs. The basic cause is an imbalance between nuclear heating and radiative cooling, which leads to the runaway of temperature-dependent thermonuclear reac-

tions [324]. There are however many aspects of burst physics that remain puzzling, such as discrepancies between predicted and observed recurrence times, and the phenomenon of burst oscillations [337, 288]. The latter are high frequency oscillations (11-600 Hz) often detected in the X-ray flux produced by thermonuclear bursts [317], and whose cause remains unknown. AMXPs can offer particular insight into burst physics and the burst oscillation mechanism, for two reasons. Firstly, they are the only sources where we have an independent measurement of the stellar spin, allowing us to measure the dependence on rotation. Secondly, they are the only sources where we can make a reasonable assessment of the effects of the magnetic field, and the role of uneven fuel distribution (due to magnetic channeling of material onto the poles of the star).

Table 5 summarizes the AMXPs that have exhibited bursts, and which of these have shown burst oscillations. Bursts are expected and observed to occur only within a range of accretion rates from $\sim 2 - 30\%$ of the Eddington rate [338, 339, 340], and in this regard the occurrence of bursts in the AMXP population accords with the behaviour seen in the non-pulsing bursters. The sources that do not show bursts are the five ultracompact sources (which are thought to have rather low accretion rates [337], likely below the minimum required for regular bursting [341]) and IGR J00291+5934, which is also thought to have a rather low accretion rate [33]. None of the AMXPs has yet shown a super-burst, longer duration bursts thought to be due to unstable carbon burning [342].

Burst properties. Bursting behaviour is known to be extremely variable, and the bursts of the AMXPs are no exception to this rule. To date there has not been a comprehensive study assessing whether the bursts from the AMXPs have properties that differ in any statistically significant way from the non-pulsing sources. However just as for the non-pulsing bursters, bursts from the AMXPs show variable recurrence times, peak fluxes and fluences, and durations, even when accretion rate seems to be relatively stable. There are nonetheless some features of AMXP bursts that are worthy of note, in particular when they are compared with bursting sources with higher magnetic fields like the mildly recycled pulsar IGR J17480–2466.

Magnetic fields and bursting. Bursts from AMXPs confirm that magnetic fields $\sim 10^8 - 10^{10}$ G (Table 1) are no impediment to thermonuclear bursting.

Burst recurrence times. Many neutron star low mass X-ray binaries show burst recurrence times of less than an hour, something that is problematic for theoretical models [343]. The only AMXP in this short recurrence time group is the highly intermittent source Aql X–1. By contrast the mildly recycled pulsar IGR J17480–2466 has the shortest recurrence time between thermonuclear bursts yet recorded, at 3.3 minutes [332], a possible sign of confined burning.

Rotation and bursting. The AMXPs, which have independent estimates of spin rate, confirm that bursting can occur for spin rates of up to a few hundred Hz (although the fastest rotating burster, 4U 1608–522, is a burst oscillation source not an accretion-powered pulsar, so the spin measure is more indirect [344]). The mildly-recycled accreting pulsar IGR J17480–2466 is instead the bursting source with burst oscil-

lations with the lowest measured rotation rate, at 11 Hz. For a star rotating at ~ 10 Hz, the Coriolis force is not dynamically relevant [53, 288], indicating that Coriolis force induced confinement of the igniting patch is not essential to the development of X-ray bursts [345] or to very short burst recurrence times (see previous point).

Cooling as a signature of thermonuclear bursts. Cooling during the tails of bursts (inferred from blackbody fits to the burst spectra) has long been regarded as a signature trait of thermonuclear Type I (rather than accretion-powered Type II) bursts. Detailed studies of the bursts from the mildly recycled pulsar IGR J17480–2466 have now shown that cooling is a sufficient but not necessary condition for the identification of thermonuclear bursts: under certain circumstances, particularly at high accretion rates, the cooling signature may not be readily detectable [333, 334, 335, 336]. Bursts from the AMXPs do however show cooling.

Marginally stable burning. The mildly recycled pulsar IGR J17480–2466 shows mHz QPOs that are interpreted as marginally stable burning of H and He on the NS surface [346, 336]. The mHz QPOs are observed when the accretion rate rises and the source transitions from unstable burning (X-ray bursts) to stable nuclear burning (no bursts). The only AMXP to have shown mHz QPOs is the highest accretion rate source, the intermittent pulsar Aql X–1 [347].

Pure helium bursts. SAX J1808.4–3658 has very bright, short bursts that are thought to be the only secure example of bursting occurring in a layer of pure helium, for a source where the accreted fuel is a mix of hydrogen and helium [85]. The only other sources that are thought to have pure helium bursts are ultra-compact sources where the donor star is too small for there to be significant hydrogen in the accreted material. Pure helium bursting is thought to occur in mixed fuel sources only in a very narrow range of accretion rates where hydrogen can burn stably to form helium before the helium ignites unstably [338].

Bursting and intermittent accretion-powered pulsations. Two of the intermittent AMXPs, HETE J1900.1–2455 and SAX J1748.9–2021, show intermittent pulsations with variable amplitudes at times when the source is also bursting [63, 45]. There does not appear to be any clear-cut causal relationship between the two phenomena (and the third intermittent AMXP, Aql X-1, does not show bursts at the time of its one intermittent pulsation episode, [42]). Nonetheless there has been speculation in the literature as to whether the two might be related. Radiation from the burst might perhaps lead to a temporary disruption of the inner edge of the disk, perturbing the flow of material onto the magnetic poles and moving the accretion footprint to a location more favorable for the formation of pulsations [311].

Burst oscillations Where the AMXPs have had the biggest impact is in our understanding of burst oscillations (see [288] for a more comprehensive review of this topic). Burst oscillations were first observed in 1996, from the non-pulsar 4U 1728–34 [348]. The oscillations manifested as a coherent signal at about 363 Hz, with an upwards drift in frequency of ~ 1 Hz as the bursts progressed, towards an asymptotic maximum in the tails. The fact that the same frequency was seen in multiple bursts

from the same source, and the stability of the asymptotic maximum frequency, suggested a link to a stable clock such as the stellar spin rate [349]. Firm identification of burst oscillation frequency with the spin frequency however had to wait until the first robust detection of burst oscillations from an AMXP [95]. Although the two frequencies appear to be very close (within a few Hz), however, the separation does differ markedly for different AMXPs. The AMXP XTE J1814–338 and the mildly recycled pulsar IGR J17480–2466 have burst oscillation frequencies that agree with the spin frequency very closely (within the error bars, $\sim 10^{-8}$ Hz for XTE J1814–338 [318, 320, 251], $\sim 10^{-4}$ Hz for IGR J17480–2466 [53]). SAX J1808.4–3658 and IGR J17511–3057, by contrast, have burst oscillations that show a rapid increase in frequency in the burst rise, slightly overshooting the spin frequency, and then stabilizing to within ~ 10 mHz of the spin frequency in the tails [95, 187]. The intermittent pulsars Aql X–1 and HETE J1900.1–2455 show burst oscillations with slow drifts throughout the bursts, more similar to those of the non-pulsars, and in these cases the asymptotic maximum frequency is ~ 1 Hz below the spin frequency [166, 350, 42, 329]. Any model for the burst oscillation mechanism must be able to explain this diversity in frequency drift and the small variations in offset from the spin frequency.

There are interesting differences in the properties of the burst oscillations from the pulsars as compared to those of the non-pulsars. For the non-pulsing bursters, burst oscillations tend only to be seen when the source is in the soft (high accretion rate) state [317]. The two intermittent pulsars conform to this rule: indeed HETE J1900.1–2455 has shown burst oscillations in only one burst, when the source entered an unusually soft state [329]. By contrast five of the six persistent pulsars with bursts have had burst oscillations in all of their bursts, even though these sources tend to be in the hard (low accretion rate) state. For the fifth, IGR J17498–2921, the data are of much poorer quality: oscillations are seen only in the brightest bursts but the upper limits on the presence of detections in the weaker bursts are comparable to the amplitudes detected in the brighter bursts [209]. The duration of burst oscillation trains also appears to differ. For SAX J1808.4–3658, XTE 1814–338 and the mildly recycled pulsar IGR J17480–2466, burst oscillations persist throughout the bursts (except during episodes of Photospheric Radius Expansion in the bright bursts from SAX 1808.4–3658). For the non-pulsars, although burst oscillations are sometimes detected throughout bursts they are more commonly detected in the tails [317], and this is also the case for the intermittent accretion-powered pulsars. In this regard the persistent pulsar IGR J17511–3057 seems to be a transitional object: at lower accretion rates oscillations are detectable throughout bursts, but as accretion rate rises the burst oscillation signal vanishes from the burst rise [187]. Burst oscillations from the pulsars have higher harmonic content than burst oscillations from the intermittent pulsars and non-pulsars [266, 95, 318, 320, 329, 187, 53]. They also have rather different amplitude-energy relations. Burst oscillations from the persistent pulsars show the same amplitude-energy relationship as their accretion-powered pulsations, irrespective of whether the latter rise or fall with energy but with the latter being more common ([95, 318, 329, 187, 53, 52, 209] and see also Section 5.1). The intermittent pulsars and non-pulsars, by contrast, have burst oscillation amplitudes that

rise with energy [351, 189]. The cause of these various differences in burst oscillation properties between the pulsars and non-pulsars remains as yet unclear, but the most obvious hypothesis is that the differences are due to the effects of a dynamically important magnetic field.

One can also use the pulsars to compare the properties of the accretion-powered pulsations (where the peak of the emission is presumed to be centered on the magnetic poles) and their burst oscillations. Burst oscillation amplitudes vary substantially from source to source, but are in most cases within a few percent of (and most lower than) the amplitude of the accretion-powered pulsations at the time of the burst [95, 318, 320, 329, 187, 53, 52]. The transitional AMXP/radio pulsar IGR J18245–2452 is an exception: for the one burst detected, the burst oscillation amplitude was much higher than the amplitude of accretion-powered pulsations immediately before the burst [12].

Pulsar burst oscillations show no statistically significant phase lags as a function of energy [351, 321, 329], unlike accretion-powered pulsations which show soft lags ([275, 352, 25, 353, 354, 186]; see also Section 5.1). Of particular interest is the strong phase-locking between accretion-powered pulsations and burst oscillations seen in XTE J1814-338 and IGR J17480-2466 [251, 53], with very small phase offset ($< 3^\circ$ and $\lesssim 10^\circ$ respectively), implying that the hot spots responsible for the two sets of pulsations are longitudinally coincident in these two sources.

So what do these results tell us about the burst oscillation mechanism? Although the mechanism is not yet understood, substantial progress has been made and the accretion-powered pulsars have played a key role. Their primary contribution, of course, has been to highlight the very close relationship between the burst oscillation frequency and the spin frequency of the star. This fact underpins the two main classes of model: hot spot models and global mode models. Small temperature variations in the surface layers mean that ignition is expected to begin at a point, with a flame front then spreading out across the star [355]. This flame may then either stall, confining the burning to a small region (the hot spot model) or excite large-scale waves in the surface layers (global mode models). The resulting temperature asymmetry gives rise to the burst oscillations. In hot spot models, the relationship with the spin rate is straightforward since the hot spot should be near stationary in the rotating frame of the star [348]. The main open theoretical question for hot spot models is what might cause the flame to stall, with both magnetic and Coriolis forces under consideration [356, 345, 53]. For global mode models, the requirement that burst oscillation frequency be very close to spin frequency puts very stringent restrictions on the types of surface modes that might be responsible [357, 358, 359]. Efforts are now ongoing to develop both classes of model to determine whether they could match the rest of the observed properties [288]. The differences between the burst oscillations from the pulsars and the non-pulsars are informative, and suggest a role for the magnetic field. What is still unclear, however, is whether we are seeing one mechanism with a continuum of properties set by stellar parameters such as the magnetic field - or whether two different mechanisms may be required. The apparent gradual changes in burst oscillation properties from the non-pulsars and intermittent pulsars (where magnetic field is likely to be weak) to the persistent pulsars (with

stronger fields) had until recently favoured the former. However new results from the pulsars point increasingly towards the possibility that we are indeed seeing two different mechanisms. The development of burst oscillations in the slowly rotating mildly recycled pulsar IGR J17480-2466 is particularly hard to understand in the context of global modes or Coriolis force induced hot spots [53]. Magnetic confinement of the flame front is at present the only plausible explanation for this source, and would also explain the extraordinary phase-locking between accretion-powered pulsations and burst oscillations. This mechanism might also operate in the other strong magnetic field source with phase-locked burst oscillations, the AMXP XTE J1814-338 [251, 53]. However for the other sources, with weaker magnetic fields, magnetic confinement is unlikely to be effective. For these sources global mode models remain a good possibility, with the differences in the pulsar burst oscillations being perhaps due to magnetic modifications to the mode structure.

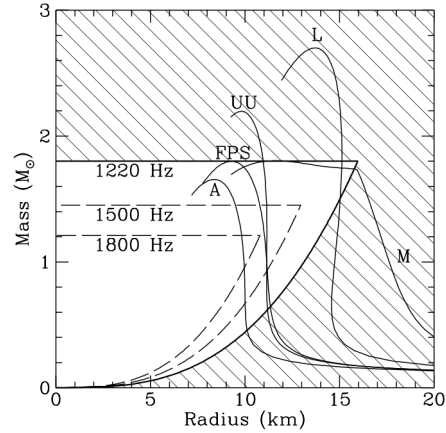
8 Aperiodic Variability and kHz QPOs

The study of aperiodic signals in power spectra of AMXPs reveals a rich phenomenology which has helped us to understand the physics of accretion disks and compact objects. All AMXPs are “atoll sources”, so-called because of their pattern in the X-ray colour-colour diagram. Atoll sources are relatively low/intermediate-luminosity LMXBs and are believed to possess low magnetic fields compared to the brightest LMXBs (the “Z sources”). The aperiodic variability of AMXPs includes phenomena at very high frequencies (the kHz QPOs) but also at lower frequency, such as the strong 1 Hz modulation observed in SAX J1808.4–3658 and NGC6440 X-2 (Sections 3.1 and 3.11). Here we highlight the main aperiodic phenomena peculiar to AMXPs and refer to Chapter 1 of this book for a more detailed discussion.

The fastest variability in LMXBs is observed as kHz QPOs, which appear at frequencies of up to ~ 1300 Hz. Sometimes two kHz QPOs are observed simultaneously as “twins”, with an “upper” QPO at frequency ν_u and a “lower” QPO at frequency ν_l . Such fast variability is observed only in LMXBs with NS accretors, and is considered to be a signature of the presence of a NS in the absence of pulsations or thermonuclear bursts. All models that try to explain kHz QPOs associate at least one of the frequencies with the orbital motion of plasma in the accretion disk. Such high frequency variability is expected given the short dynamical timescale (0.1-1 ms) characterizing the motion of matter near NSs. Such rapid variability is never observed in black hole LMXBs⁴, possibly because they have larger mass and hence a larger innermost stable circular orbit (ISCO). The ISCO is a limiting radius (at $6GM/c^2$ for non-rotating NSs) set by General Relativity that defines the smallest stable orbit in an accretion disk. The frequency of kHz QPOs is close to the value expected for stable Keplerian orbits around a NS, and can therefore be used to place constraints on the mass and radius of the NS (and hence the EoS of ultra-dense mat-

⁴ Fast variability appears in black hole LMXBs below ~ 500 Hz as “high frequency QPOs”.

Fig. 10 Constraints on the Mass-Radius relation of NSs from kHz QPOs. The solid curves refer to a sample of different EoS models (for non-rotating NSs), and the thick solid and dashed lines enclose regions of the M-R diagram compatible with the observation of kHz QPOs at a certain Keplerian frequency (image from [360]).



ter). The size of the orbit where kHz QPOs are produced must be larger than both NS radius and ISCO, both of which depend on NS mass (Figure 10).

The four AMXPs with twin kHz QPOs (SAX J1808.4–3658, XTE J1807–294, IGR J17511–305 and Aql X-1; Section 3) have been used to test kHz QPO formation models (e.g., the rejection of the beat-frequency model; Section 3.1) and have illuminated the relation with the NS spin. Taking into account also the NXPs with twin kHz QPOs, it is clear that the relation between kHz QPO separation $\Delta\nu = \nu_u - \nu_l$ and spin frequency ν_s is not as simple as originally thought: $\Delta\nu/\nu_s$ is not always equal to 1 or 0.5. $\Delta\nu$ and ν_s may even be unrelated: instead we see an average $\langle\Delta\nu\rangle \approx 300$ Hz for all sources *except* AMXPs [361, 362]. *Only* for the AMXPs, where the magnetic field is strong enough to channel accretion, is the ratio $\Delta\nu/\nu_s$ either 1 or 0.5. Some predictions of the sonic-point spin resonance and relativistic-resonance models [363, 364] are consistent with the AMXP results. In sonic-point spin resonance models, the magnetic and radiation fields rotating with the star excite a vertical motion of the disk gas at the “spin-resonance” radius r_{sr} . There, the vertical epicyclic frequency equals the difference between the orbital frequency and the spin. Depending on the “clumpiness” of the flow at r_{sr} , the X-ray flux exhibits $\Delta\nu$ equal to either ν_s (smooth flow) or $0.5\nu_s$ (clumpy flow). In relativistic resonance models, a non-linear 1:2 or 1:3 resonance between orbital and radial epicyclic motion emerges as a consequence of the deviation of the strong gravitational potential from the Newtonian $1/r$. A third model suggests that kHz QPOs are related to the three general relativistic epicyclic frequencies [365] or to the precession of frame dragging (Lense-Thirring precession [366]). So far none of these models satisfactorily accounts for all of the rich phenomenology of kHz QPOs.

Determining the origin of QPOs, in particular kHz QPOs is of fundamental importance as this is a phenomenon that is common in LMXBs. If a clear relation with the NS mass and/or radius is confirmed, it has the potential to place severe constraints on the EoS of ultra-dense matter. This field has however seen few advancements in the past few years, at least on the theoretical side. New attempts are

now using numerical simulations to interpret the observations and test some of the original models [367, 368, 369, 252]. Most of these simulations use black hole accretors (but see [252]) which do not have kHz QPOs, but the results are promising in terms of understanding the generation of variability in LMXBs as a whole.

9 Open Problems and Final Remarks

Since the first discovery in 1998, the AMXPs have provided an incredibly body of observational data allowing us to understand NSs and their evolution. They have allowed the study of extreme phenomena on the surface of the NSs, in the strong gravity regime at relativistic rotational velocities, and have helped us to understand how radio pulsars form and evolve within the framework of the *recycling scenario*.

Proposed X-ray missions like the Indian *ASTROSAT*, the NASA *AXTAR* satellite and the ESA missions *LOFT* and *Athena+* will guarantee huge advances in our knowledge of these systems, building on the extraordinary results from *RXTE*, *XMM-Newton*, *Chandra* and *Swift*. Long-term monitoring of future AMXP outbursts will allow measurement of long-term spin and orbital behaviour, something that has at present only been done for four systems. Increased collecting area will increase sensitivity to pulsations by orders of magnitude, leading (we hope) to the discovery of sub-millisecond pulsars or strengthening the 730 Hz spin distribution cutoff. In the former case this would place very tight constraints on the EoS of ultra-dense matter. Modeling of high signal to noise pulse profiles will reveal the subtle features imparted by strong gravity, enabling us to measure the NS compactness. We will be able to test models for kHz QPOs and burst oscillations with sufficient precision that we can finally determine the underpinning mechanism.

Of the many open problems, there are several that stand out. One big mystery is why do so very few LMXBs show pulsations? If magnetic field evolution and decay is involved, we may finally be able to understand the origin and the evolution of nature's strongest magnetic fields. What happens when accretion takes place during an outburst? Why we do not detect the effect of accretion torques in some AMXPs, contrary to expectations? Are gravitational waves involved as a braking mechanism that counteracts the effect of accretion or are we again missing some fundamental ingredient? When do accreting pulsars switch on as radio pulsars? Are all AMXPs turning on as radio millisecond pulsars during quiescence? What is the relation between AMXPs and the radio pulsar "black-widows" and "red-backs"? We look forward to discovering the answers to these questions in the years ahead.

Acknowledgements We would like to thank C. Heinke, J. Poutanen, R. Lovelace, M. Linares, T. Tauris, D. Altamirano, B. Haskell, P. D'Avanzo, D. Bhattacharya, J. Hessels and N. Masetti for providing useful comments and suggestions. We acknowledge support from an NWO Veni (AP) & Vidi (AP, AW) fellowships.

References

1. Hewish, A., Bell, S. J., Pilkington, J. D. H., Scott, P. F., & Collins, R. A. 1968, *Nature*, 217, 709
2. D.C. Backer, S.R. Kulkarni, C. Heiles, M.M. Davis, W.M. Goss, *Nature* **300**, 615 (1982)
3. M.A. Alpar, A.F. Cheng, M.A. Ruderman, J. Shaham, *Nature* **300**, 728 (1982)
4. V. Radhakrishnan, G. Srinivasan, *Current Science* **51**, 1096 (1982)
5. G. Srinivasan, *New Astronomy Reviews* **54**, 93 (2010)
6. D. Bhattacharya, E.P.J. van den Heuvel, *Phys. Rep.* **203**, 1 (1991)
7. T.M. Tauris, E.P.J. van den Heuvel, *Formation and evolution of compact stellar X-ray sources* (Compact stellar X-ray sources, 2006), pp. 623–665
8. R. Wijnands, M. van der Klis, *Nature* **394**, 344 (1998)
9. B.W. Stappers, A. Archibald, C. Bassa, J. Hessels, G. Janssen, V. Kaspi, A. Lyne, A. Patruno, A.B. Hill, *ATel* **5513**, 1 (2013)
10. A. Patruno, A.M. Archibald, J.W.T. Hessels, S. Bogdanov, B.W. Stappers, C.G. Bassa, G.H. Janssen, V.M. Kaspi, S. Tendulkar, A.G. Lyne, arXiv:1310.7549 (2013)
11. A.M. Archibald, I.H. Stairs, et al., *Science* **324**, 1411 (2009)
12. A. Papitto, C. Ferrigno, et al., *Nature* **501**, 517 (2013)
13. L. Bildsten, *ApJ* **577**, L27 (2002)
14. L.A. Nelson, S. Rappaport, *ApJ* **598**, 431 (2003)
15. C.J. Deloye, L. Bildsten, *ApJ* **598**, 1217 (2003)
16. A. Patruno, M.A. Alpar, M. van der Klis, E.P.J. van den Heuvel, *ApJ* **752**, 33 (2012)
17. A. Patruno, P. Bult, A. Gopakumar, J.M. Hartman, R. Wijnands, M. van der Klis, D. Chakrabarty, *ApJ* **746**, L27 (2012)
18. J.M. Hartman, A. Patruno, D. Chakrabarty, D.L. Kaplan, C.B. Markwardt, E.H. Morgan, P.S. Ray, M. van der Klis, R. Wijnands, *ApJ* **675**, 1468 (2008)
19. J.M. Hartman, A. Patruno, D. Chakrabarty, C.B. Markwardt, E.H. Morgan, M. van der Klis, R. Wijnands, *ApJ* **702**, 1673 (2009)
20. A. Papitto, T. di Salvo, A. D’Aì, R. Iaria, L. Burderi, A. Riggio, M.T. Menna, N.R. Robba, *A&A* **493**, L39 (2009)
21. E.M. Cackett, D. Altamirano, A. Patruno, J.M. Miller, M. Reynolds, M. Linares, R. Wijnands, *ApJ* **694**, L21 (2009)
22. C.B. Markwardt, J.H. Swank, T.E. Strohmayer, J.J.M.i. Zand, F.E. Marshall, *ApJ* **575**, L21 (2002)
23. A. Papitto, M.T. Menna, L. Burderi, T. di Salvo, A. Riggio, *MNRAS* **383**, 411 (2008)
24. R.A. Remillard, J. Swank, T. Strohmayer, *IAU Circ.* **7893**, 1 (2002)
25. D.K. Galloway, D. Chakrabarty, E.H. Morgan, R.A. Remillard, *ApJ* **576**, L137 (2002)
26. C.B. Markwardt, E. Smith, J.H. Swank, *IAU Circ.* **8080** (2003)
27. M.G.F. Kirsch, K. Mukerjee, M.G. Breitfellner, S. Djavidnia, M.J. Freyberg, E. Kendziorra, M.J.S. Smith, *A&A* **423**, L9 (2004)
28. Y. Chou, Y. Chung, C.P. Hu, T.C. Yang, *ApJ* **678**, 1316 (2008)
29. A. Riggio, T. Di Salvo, L. Burderi, M.T. Menna, A. Papitto, R. Iaria, G. Lavagetto, *ApJ* **678**, 1273 (2008)
30. A. Patruno, J.M. Hartman, R. Wijnands, D. Chakrabarty, M. van der Klis, *ApJ* **717**, 1253 (2010)
31. C.B. Markwardt, J.H. Swank, *IAU Circ.* **8144**, 1 (2003)
32. A. Papitto, T. di Salvo, L. Burderi, M.T. Menna, G. Lavagetto, A. Riggio, *MNRAS* **375**, 971 (2007)
33. D.K. Galloway, C.B. Markwardt, E.H. Morgan, D. Chakrabarty, T.E. Strohmayer, *ApJ* **622**, L45 (2005)
34. M. Falanga, L. Kuiper, J. Poutanen, E.W. Bonning, W. Hermsen, T. di Salvo, P. Goldoni, A. Goldwurm, S.E. Shaw, L. Stella, *A&A* **444**, 15 (2005)
35. L. Burderi, T. Di Salvo, G. Lavagetto, M.T. Menna, A. Papitto, A. Riggio, R. Iaria, F. D’Antona, N.R. Robba, L. Stella, *ApJ* **657**, 961 (2007)

36. A. Patruno, *ApJ* **722**, 909 (2010)
37. J.M. Hartman, D.K. Galloway, D. Chakrabarty, *ApJ* **726**, 26 (2011)
38. A. Papitto, A. Riggio, L. Burderi, T. di Salvo, A. D'Ai, R. Iaria, *A&A* **528**, A55 (2011)
39. P. Kaaret, E.H. Morgan, R. Vanderspek, J.A. Tomsick, *ApJ* **638**, 963 (2006)
40. H.A. Krimm, C.B. Markwardt, C.J. Deloye, P. Romano, D. Chakrabarty, S. Campana, J.R. Cummings, D.K. Galloway, N. Gehrels, J.M. Hartman, P. Kaaret, E.H. Morgan, J. Tueller, *ApJ* **668**, L147 (2007)
41. A. Patruno, D. Altamirano, C. Messenger, *MNRAS* **403**, 1426 (2010)
42. P. Casella, D. Altamirano, A. Patruno, R. Wijnands, M. van der Klis, *ApJ* **674**, L41 (2008)
43. W.F. Welsh, E.L. Robinson, P. Young, *AJ* **120**, 943 (2000)
44. A. Patruno, D. Altamirano, J.W.T. Hessels, P. Casella, R. Wijnands, M. van der Klis, *ApJ* **690**, 1856 (2009)
45. D. Altamirano, P. Casella, A. Patruno, R. Wijnands, M. van der Klis, *ApJ* **674**, L45 (2008)
46. D. Altamirano, A. Patruno, C.O. Heinke, C. Markwardt, T.E. Strohmayer, M. Linares, R. Wijnands, M. van der Klis, J.H. Swank, *ApJ* **712**, L58 (2010)
47. C.B. Markwardt, D. Altamirano, J.H. Swank, T.E. Strohmayer, M. Linares, D. Pereira, *ATel* **2197**, 1 (2009)
48. A. Riggio, A. Papitto, L. Burderi, T. di Salvo, M. Bachetti, R. Iaria, A. D'Ai, M.T. Menna, *A&A* **526**, A95 (2011)
49. D. Altamirano, Y. Cavecchi, A. Patruno, A. Watts, M. Linares, N. Degenaar, M. Kalamkar, M. van der Klis, N. Rea, P. Casella, M. Armas Padilla, R. Kaur, Y.J. Yang, P. Soleri, R. Wijnands, *ApJ* **727**, L18 (2011)
50. A. Papitto, A. D'Ai, S. Motta, A. Riggio, L. Burderi, T. di Salvo, T. Belloni, R. Iaria, *A&A* **526**, L3 (2011)
51. T.E. Strohmayer, C.B. Markwardt, *ATel* **2929**, 1 (2010)
52. A. Papitto, T. di Salvo, L. Burderi, M.T. Menna, G. Lavagetto, A. Riggio, *MNRAS* **375**, 971 (2007)
53. Y. Cavecchi, A. Patruno, B. Haskell, A.L. Watts, Y. Levin, M. Linares, D. Altamirano, R. Wijnands, M. van der Klis, *ApJ* **740**, L8 (2011)
54. P.G. Jonker, M. van der Klis, *ApJ* **553**, L43 (2001)
55. L. Bildsten, E.F. Brown, *ApJ* **477**, 897 (1997)
56. A. Levine, C.P. Ma, J. McClintock, S. Rappaport, M. van der Klis, F. Verbunt, *ApJ* **327**, 732 (1988)
57. W. Coburn, W.A. Heindl, R.E. Rothschild, D.E. Gruber, I. Kreykenbohm, J. Wilms, P. Kretschmar, R. Staubert, *ApJ* **580**, 394 (2002)
58. W. Cui, *ApJ* **482**, L163 (1997)
59. W. Zhang, E.H. Morgan, K. Jahoda, J.H. Swank, T.E. Strohmayer, G. Jernigan, R.I. Klein, *ApJ* **469**, L29 (1996)
60. K.H. Hinkle, F.C. Fekel, R.R. Joyce, P.R. Wood, V.V. Smith, T. Lebzelter, *ApJ* **641**, 479 (2006)
61. K. Postnov, N. Shakura, et al., in *Proceedings of the 8th INTEGRAL Workshop "The Restless Gamma-ray Universe"*. September 27-30 2010. Dublin, Ireland. (2010)
62. R.H.D. Corbet, J.L. Sokoloski, K. Mukai, C.B. Markwardt, J. Tueller, *ApJ* **675**, 1424 (2008)
63. D.K. Galloway, E.H. Morgan, M.I. Krauss, P. Kaaret, D. Chakrabarty, *ApJ* **654**, L73 (2007)
64. A. Patruno, *ApJL*, in press (2012)
65. A. Patruno, D. Altamirano, et al., *ATel* **2407**, 1 (2010)
66. M.A.P. Torres, P.G. Jonker, D. Steeghs, G.H.A. Roelofs, J.S. Bloom, J. Casares, E.E. Falco, M.R. Garcia, T.R. Marsh, M. Mendez, J.M. Miller, G. Nelemans, P. Rodríguez-Gil, *ApJ* **672**, 1079 (2008)
67. M.I. Krauss, Z. Wang, A. Dullighan, A.M. Juett, D.L. Kaplan, D. Chakrabarty, M.H. van Kerkwijk, D. Steeghs, P.G. Jonker, C.B. Markwardt, *ApJ* **627**, 910 (2005)
68. A.B. Giles, J.G. Greenhill, K.M. Hill, E. Sanders, *MNRAS* **361**, 1180 (2005)
69. V. Tudose, Z. Paragi, J. Yang, J.C.A. Miller-Jones, R. Fender, M. Garrett, A. Rushton, R. Spencer, *ATel* **5158**, 1 (2013)

70. D. Pooley, W.H.G. Lewin, F. Verbunt, L. Homer, B. Margon, B.M. Gaensler, V.M. Kaspi, J.M. Miller, D.W. Fox, M. van der Klis, *ApJ* **573**, 184 (2002)
71. C.O. Heinke, D. Altamirano, et al., *ApJ* **714**, 894 (2010)
72. P. D'Avanzo, S. Campana, T. Muñoz-Darias, T. Belloni, E. Bozzo, M. Falanga, L. Stella, *A&A* **534**, A92 (2011)
73. M.A. Nowak, A. Paizis, J. Wilms, J. Rodriguez, S. Chaty, K. Ebisawa, M. Del Santo, R. Farinelli, P. Ubertini, T. Courvoisier, *ATel* **2215**, 1 (2009)
74. D. Chakrabarty, C.B. Markwardt, M. Linares, P.G. Jonker, *ATel* **3606**, 1 (2011)
75. D.B. Fox, *ATel* **526**, 1 (2005)
76. L. Pavan, G. Wong, M.H. Wieringa, N.F.H. Tothill, M.D. Filipovic, E. Bozzo, C. Ferrigno, A. Papitto, P. Romano, *ATel* **4981**, 1 (2013)
77. J.J.M. in 't Zand, J. Heise, J.M. Muller, A. Bazzano, M. Cocchi, L. Natalucci, P. Ubertini, *A&A* **331**, L25 (1998)
78. J.J.M. in't Zand, R. Cornelisse, E. Kuulkers, J. Heise, L. Kuiper, A. Bazzano, M. Cocchi, J.M. Muller, L. Natalucci, M.J.S. Smith, P. Ubertini, *A&A* **372**, 916 (2001)
79. D. Chakrabarty, E.H. Morgan, *Nature* **394**, 346 (1998)
80. L. Bildsten, D. Chakrabarty, *ApJ* **557**, 292 (2001)
81. R. Wijnands, M. Méndez, C. Markwardt, M. van der Klis, D. Chakrabarty, E. Morgan, *ApJ* **560**, 892 (2001)
82. R. Wijnands, *ApJ* **588**, 425 (2003)
83. A. Patruno, A. Watts, M. Klein Wolt, R. Wijnands, M. van der Klis, *ApJ* **707**, 1296 (2009)
84. J.P. Lasota, *New Astronomy Review* **45**, 449 (2001)
85. D.K. Galloway, A. Cumming, *ApJ* **652**, 559 (2006)
86. M. van der Klis, D. Chakrabarty, J.C. Lee, E.H. Morgan, R. Wijnands, C.B. Markwardt, J.H. Swank, *IAU Circ.* **7358**, 3 (2000)
87. H.C. Spruit, R.E. Taam, *ApJ* **402**, 593 (1993)
88. C.R. D'Angelo, H.C. Spruit, *MNRAS* **406**, 1208 (2010)
89. R. Wijnands, M. van der Klis, J. Homan, D. Chakrabarty, C.B. Markwardt, E.H. Morgan, *Nature* **424**, 44 (2003)
90. P.G. Jonker, M. Méndez, M. van der Klis, *ApJ* **540**, L29 (2000)
91. M. Gilfanov, M. Revnivtsev, R. Sunyaev, E. Churazov, *A&A* **338**, L83 (1998)
92. M. Gierliński, C. Done, D. Barret, *MNRAS* **331**, 141 (2002)
93. A. Patruno, N. Rea, D. Altamirano, M. Linares, R. Wijnands, M. van der Klis, *MNRAS* **396**, L51 (2009)
94. A. Ibragimov, J. Poutanen, *MNRAS* **400**, 492 (2009)
95. D. Chakrabarty, E.H. Morgan, M.P. Muno, D.K. Galloway, R. Wijnands, M. van der Klis, C.B. Markwardt, *Nature* **424**, 42 (2003)
96. E. Kuulkers, P.R. den Hartog, J.J.M. in't Zand, F.W.M. Verbunt, W.E. Harris, M. Cocchi, *A&A* **399**, 663 (2003)
97. P. Roche, D. Chakrabarty, L. Morales-Rueda, R. Hynes, S.M. Slivan, C. Simpson, P. Hewett, *IAU Circ.* **6885** (1998)
98. A.B. Giles, K.M. Hill, J.G. Greenhill, *MNRAS* **304**, 47 (1999)
99. Z. Wang, D. Chakrabarty, P. Roche, P.A. Charles, E. Kuulkers, T. Shahbaz, C. Simpson, D.A. Forbes, S.F. Helsdon, *ApJ* **563**, L61 (2001)
100. Greenhill, J. G., Giles, A. B., & Coutures, C. 2006, *MNRAS*, 370, 1303
101. Rupen, M. P., Dhawan, V., & Mioduszewski, A. J. 2005, *The Astronomer's Telegram*, 524, 1
102. L. Homer, P.A. Charles, D. Chakrabarty, L. van Zyl, *MNRAS* **325**, 1471 (2001)
103. C.J. Deloye, C.O. Heinke, R.E. Taam, P.G. Jonker, *MNRAS* **391**, 1619 (2008)
104. Z. Wang, R.P. Breton, C.O. Heinke, C.J. Deloye, J. Zhong, *ApJ* **765**, 151 (2013)
105. Z. Wang, C. Bassa, A. Cumming, V.M. Kaspi, *ApJ* **694**, 1115 (2009)
106. L. Burderi, T. Di Salvo, F. D'Antona, N.R. Robba, V. Testa, *A&A* **404**, L43 (2003)
107. S. Campana, P. D'Avanzo, J. Casares, S. Covino, G. Israel, G. Marconi, R. Hynes, P. Charles, L. Stella, *ApJ* **614**, L49 (2004)
108. M.N. Iacolina, M. Burgay, L. Burderi, A. Possenti, T. di Salvo, *A&A* **519**, A13 (2010)
109. S. Rappaport, P.C. Joss, R.F. Webbink, *ApJ* **254**, 616 (1982)

110. S.A. Grebenev, S.V. Molkov, R.A. Sunyaev, *ATel* **446**, 1 (2005)
111. J.H. Swank, C.B. Markwardt, E.A. Smith, *ATel* **449**, 1 (2005)
112. C.B. Markwardt, J.H. Swank, *ATel* **1045**, 1 (2007)
113. C.B. Markwardt, D. Pereira, J.H. Swank, *ATel* **1051**, 1 (2007)
114. J. Chenevez, E. Kuulkers, et al., *ATel* **2235**, 1 (2009)
115. C.B. Markwardt, D. Altamirano, T.E. Strohmayer, J.H. Swank, *ATel* **2237**, 1 (2009)
116. J.M. Miller, R. Wijnands, M. Méndez, E. Kendziorra, A. Tiengo, M. van der Klis, D. Chakrabarty, B.M. Gaensler, W.H.G. Lewin, *ApJ* **583**, L99 (2003)
117. M. Gierliński, J. Poutanen, *MNRAS* **359**, 1261 (2005)
118. P.G. Jonker, G. Nelemans, et al., *MNRAS* **344**, 201 (2003)
119. R.A. Remillard, J. Swank, T. Strohmayer, *IAU Circ.* **7893** (2002)
120. A.J. Castro-Tirado, A. Caccianiga, J. Gorosabel, P. Kilmartin, P. Tristram, P. Yock, C. Sanchez-Fernandez, M.E. Alcoholado-Feltstrom, *IAU Circ.* **7895**, 1 (2002)
121. A.M. Juett, D.K. Galloway, D. Chakrabarty, *ApJ* **587**, 754 (2003)
122. J.G. Greenhill, A.B. Giles, K.M. Hill, *IAU Circ.* **7889**, 1 (2002)
123. G. Nelemans, P.G. Jonker, D. Steeghs, *MNRAS* **370**, 255 (2006)
124. M.P. Rupen, V. Dhawan, A.J. Mioduszewski, *IAU Circ.* **7893**, 2 (2002)
125. M. Monelli, G. Fiorentino, L. Burderi, F. D'Antona, N. Robba, V. Testa, in *Interacting Binaries: Accretion, Evolution, and Outcomes*, American Institute of Physics Conference Series, vol. 797, pp. 565–568, ed. by L. Burderi, et al. (2005)
126. P. D'Avanzo, S. Campana, J. Casares, S. Covino, G.L. Israel, L. Stella, *A&A* **508**, 297 (2009)
127. M. Falanga, J.M. Bonnet-Bidaud, J. Poutanen, R. Farinelli, A. Martocchia, P. Goldoni, J.L. Qu, L. Kuiper, A. Goldwurm, *A&A* **436**, 647 (2005)
128. M. Linares, M. van der Klis, D. Altamirano, C.B. Markwardt, *ApJ* **634**, 1250 (2005)
129. R. Wijnands, A. Reynolds, *ATel* **166**, 1 (2003)
130. M.I. Krauss, A. Dullighan, D. Chakrabarty, M.H. van Kerkwijk, C.B. Markwardt, *IAU Circ.* **8154**, 3 (2003)
131. D. Steeghs, *IAU Circ.* **8155**, 2 (2003)
132. M.C. Baglio, P. D'Avanzo, T. Muñoz-Darias, R.P. Breton, S. Campana, *A&A* **559**, A42 (2013)
133. D. Eckert, R. Walter, P. Kretschmar, M. Mas-Hesse, G.G.C. Palumbo, J.P. Roques, P. Ubertini, C. Winkler, *ATel* **352**, 1 (2004)
134. C.B. Markwardt, J.H. Swank, T.E. Strohmayer, *ATel* **353**, 1 (2004)
135. C.B. Markwardt, D.K. Galloway, D. Chakrabarty, E.H. Morgan, T.E. Strohmayer, *ATel* **360**, 1 (2004)
136. D. Chakrabarty, J.H. Swank, C.B. Markwardt, E. Smith, *ATel* **1660**, 1 (2008)
137. F. Lewis, D.M. Russell, et al., *A&A* **517**, A72 (2010)
138. P.G. Jonker, M.A.P. Torres, D. Steeghs, *ApJ* **680**, 615 (2008)
139. R. Remillard, *ATel* **357**, 1 (2004)
140. A. Paizis, M.A. Nowak, J. Wilms, T. J-L. Courvoisier, K. Ebisawa, J. Rodriguez, P. Ubertini, *A&A* **444**, 357 (2005)
141. D.B. Fox, S.R. Kulkarni, *ATel* **354**, 1 (2004)
142. G. Roelofs, P.G. Jonker, D. Steeghs, M. Torres, G. Nelemans, *ATel* **356**, 1 (2004)
143. P. D'Avanzo, S. Campana, S. Covino, G.L. Israel, L. Stella, G. Andreuzzi, *A&A* **472**, 881 (2007)
144. G. Pooley, *ATel* **355**, 1 (2004)
145. R. Fender, G. De Bruyn, G. Pooley, B. Stappers, *ATel* **361**, 1 (2004)
146. M. Linares, V. Tudose, S. Migliari, *ATel* **1667**, 1 (2008)
147. R. Vanderspek, E. Morgan, G. Crew, C. Graziani, M. Suzuki, *ATel* **516**, 1 (2005)
148. E. Morgan, P. Kaaret, R. Vanderspek, *ATel* **523**, 1 (2005)
149. N. Kawai, M. Suzuki, *ATel* **534**, 1 (2005)
150. M. Suzuki, N. Kawai, et al., *PASJ* **59**, 263 (2007)
151. M. Falanga, L. Titarchuk, *ApJ* **661**, 1084 (2007)
152. D.K. Galloway, in *The Transient Milky Way: A Perspective for MIRAX*, *AIPC*, vol. 840, ed. by F. D'Amico, J. Braga, & R. E. Rothschild (2006), *AIPC*, vol. 840, pp. 50–54

153. D.K. Galloway, E.H. Morgan, D. Chakrabarty, in *A Decade of Accreting Millisecond X-Ray Pulsars, AIPC Series*, vol. 1068, pp. 55–62, ed. by R. Wijnands et al. (2008)
154. D. Steeghs, M.A.P. Torres, C. Blake, J.S. Bloom, *ATel* **533**, 1 (2005)
155. D. Steeghs, M.A.P. Torres, M.R. Garcia, J.E. McClintock, J.M. Miller, P.G. Jonker, P.J. Callanan, P. Zhao, P. Berlind, R. Hutchins, C. Watson, *ATel* **543**, 1 (2005)
156. N. Degenaar, R. Wijnands, S. Campana, D. Galloway, W. Lewin, J. Homan, D. Chakrabarty, P. Jonker, E. Cackett, J. Miller, *ATel* **1098**, 1 (2007)
157. M.A.P. Torres, P. Rodriguez-Gil, D. Steeghs, J.M. Corral-Santana, J. Casares, P.G. Jonker, *ATel* **1090**, 1 (2007)
158. P. Elebert, P.J. Callanan, A.V. Filippenko, P.M. Garnavich, G. Mackie, J.M. Hill, V. Burwitz, *MNRAS* **383**, 1581 (2008)
159. M.P. Rupen, A.J. Mioduszewski, V. Dhawan, *ATel* **530**, 1 (2005)
160. C.B. Markwardt, H.A. Krimm, J.H. Swank, *ATel* **1108** (2007)
161. A. Patruno, C.B. Markwardt, T.E. Strohmayer, J.H. Swank, S.E. Smith, D. Pereira, *ATel* **2130**, 1 (2009)
162. L. Burderi, V. Testa, et al., *ATel* **1132**, 1 (2007)
163. A. Possenti, M. Murgia, et al., *ATel* **1128**, 1 (2007)
164. J.W.T. Hessels, B.W. Stappers, *ATel* **1129**, 1 (2007)
165. A. Papitto, T. di Salvo, et al., *ATel* **1133**, 1 (2007)
166. W. Zhang, K. Jahoda, R.L. Kelley, T.E. Strohmayer, J.H. Swank, S.N. Zhang, *ApJ* **495**, L9+ (1998)
167. D. Barret, M. Boutelier, M.C. Miller, *MNRAS* **384**, 1519 (2008)
168. J. Thorstensen, P. Charles, S. Bowyer, *ApJ* **220**, L131 (1978)
169. C. Chevalier, S.A. Ilovaisky, P. Leisy, F. Patat, *A&A* **347**, L51 (1999)
170. C. Chevalier, S.A. Ilovaisky, *A&A* **251**, L11 (1991)
171. R.M. Hjellming, X. Han, D. Roussel-Dupre, *IAU Circ.* **5112**, 1 (1990)
172. M.P. Rupen, A.J. Mioduszewski, V. Dhawan, *ATel* **286**, 1 (2004)
173. M.P. Rupen, A.J. Mioduszewski, V. Dhawan, *ATel* **491**, 1 (2005)
174. J.C.A. Miller-Jones, G.R. Sivakoff, et al., *ApJ* **716**, L109 (2010)
175. J.J.M. in 't Zand, F. Verbunt, T.E. Strohmayer, A. Bazzano, M. Cocchi, J. Heise, M.H. van Kerkwijk, J.M. Muller, L. Natalucci, M.J.S. Smith, P. Ubertini, *A&A* **345**, 100 (1999)
176. F. Verbunt, M.H. van Kerkwijk, J.J.M. in 't Zand, J. Heise, *A&A* **359**, 960 (2000)
177. S. Ortolani, B. Barbuy, E. Bica, *A&AS* **108**, 653 (1994)
178. F.P. Gavriil, T.E. Strohmayer, J.H. Swank, C.B. Markwardt, in *AAS/High Energy Astrophysics Division #9, Bulletin of the American Astronomical Society*, vol. 38, p. 336, (2006)
179. F.P. Gavriil, T.E. Strohmayer, J.H. Swank, C.B. Markwardt, *ApJ* **669**, L29 (2007)
180. E.M. Cackett, R. Wijnands, C.O. Heinke, P.D. Edmonds, W.H.G. Lewin, D. Pooley, J.E. Grindlay, P.G. Jonker, J.M. Miller, *ApJ* **620**, 922 (2005)
181. J.J.M. in 't Zand, M.H. van Kerkwijk, D. Pooley, F. Verbunt, R. Wijnands, W.H.G. Lewin, *ApJ* **563**, L41 (2001)
182. J.C.A. Miller-Jones, C.O. Heinke, G.R. Sivakoff, D. Pooley, J. Homan, D. Altamirano, *ATel* **2377**, 1 (2010)
183. C.O. Heinke, S.A. Budac, *ATel* **2139**, 1 (2009)
184. A. Patruno, C. D'Angelo, *ApJ* **771**, 94 (2013)
185. C. Baldovin, E. Kuulkers, et al., *ATel* **2196**, 1 (2009)
186. A. Papitto, A. Riggio, T. di Salvo, L. Burderi, A. D'Ai, R. Iaria, E. Bozzo, M.T. Menna, *MNRAS* **407**, 2575 (2010)
187. D. Altamirano, A. Watts, M. Linares, C.B. Markwardt, T. Strohmayer, A. Patruno, *MNRAS* **409**, 1136 (2010)
188. E. Bozzo, C. Ferrigno, M. Falanga, S. Campana, J.A. Kennea, A. Papitto, *A&A* **509**, L3 (2010)
189. A.L. Watts, D. Altamirano, C.B. Markwardt, T.E.S. ., *ATel* **2199**, 1 (2009)
190. A. Ibragimov, J.J.E. Kajava, J. Poutanen, *MNRAS* **415**, 1864 (2011)
191. M. Falanga, L. Kuiper, J. Poutanen, D.K. Galloway, E.W. Bonning, E. Bozzo, A. Goldwurm, W. Hermsen, L. Stella, *A&A* **529**, A68 (2011)

192. M. Kalamkar, D. Altamirano, M. van der Klis, *ApJ* **729**, 9 (2011)
193. M.A.P. Torres, P.G. Jonker, D. Steeghs, I. Damjanov, E. Caris, K. Glazebrook, *ATel* **2233**, 1 (2009)
194. J.C.A. Miller-Jones, D.M. Russell, S. Migliari, *ATel* **2232**, 1 (2009)
195. P. Schady, A.P. Beardmore, F.E. Marshall, D.M. Palmer, E. Rol, G. Sato, GRB Coordinates Network **5200**, 1 (2006)
196. R. Wijnands, E. Rol, E. Cackett, R.L.C. Starling, R.A. Remillard, *MNRAS* **393**, 126 (2009)
197. J. Halpern, GRB Coordinates Network **5210**, 1 (2006)
198. L. Pavan, J. Chenevez, et al., *ATel* **2548**, 1 (2010)
199. J. Chenevez, E. Kuulkers, et al., *ATel* **2924**, 1 (2010)
200. D. Altamirano, R. Wijnands, et al., *ATel* **2565**, 1 (2010)
201. E. Bozzo, T. Belloni, G. Israel, L. Stella, *ATel* **2567**, 1 (2010)
202. T. Belloni, L. Stella, E. Bozzo, G. Israel, S. Campana, *ATel* **2568**, 1 (2010)
203. T.E. Strohmayer, C.B. Markwardt, *ATel* **2569**, 1 (2010)
204. C.B. Markwardt, T.E. Strohmayer, *ApJ* **717**, L149 (2010)
205. C. Ferrigno, E. Bozzo, M. Falanga, L. Stella, S. Campana, T. Belloni, G.L. Israel, L. Pavan, E. Kuulkers, A. Papitto, *A&A* **525**, A48 (2011)
206. L. Gibaud, A. Bazzano, et al., *ATel* **3551**, 1 (2011)
207. C. Ferrigno, E. Bozzo, L.G.A.P.T.M. Belloni, *ATel* **3560**, 1 (2011)
208. M. Linares, D. Altamirano, et al., *ATel* **3568**, 1 (2011)
209. M. Chakraborty, S. Bhattacharyya, *MNRAS* **422**, 2351 (2012)
210. M. Linares, E. Bozzo, et al., *ATel* **3661**, 1 (2011)
211. S. Greiss, D. Steeghs, T. Maccarone, P.G. Jonker, M.A.P. Torres, O. Gonzalez, N. Masetti, A. Rojas, *ATel* **3562**, 1 (2011)
212. D.M. Russell, F. Lewis, D. Altamirano, P. Roche, *ATel* **3622**, 1 (2011)
213. M. van den Berg, J. Grindlay, P. Zhao, J. Hong, M. Servillat, *ATel* **3634**, 1 (2011)
214. M.A.P. Torres, O. Madej, P.G. Jonker, D. Steeghs, S. Greiss, N. Morrell, M. Roth, *ATel* **3638**, 1 (2011)
215. D. Eckert, M. Del Santo, A. Bazzano, K. Watanabe, A. Paizis, E. Bozzo, C. Ferrigno, I. Caballero, L. Sidoli, L. Kuiper, *ATel* **4925**, 1 (2013)
216. C.O. Heinke, A. Bahramian, R. Wijnands, D. Altamirano, *ATel* **4927**, 1 (2013)
217. C. Ferrigno, E. Bozzo, A. Papitto, N. Rea, L. Pavan, S. Campana, M. Wieringa, M. Filipovic, M. Falanga, arXiv:1310.7784 (2013)
218. M. Linares, A. Bahramian, C. Heinke, R. Wijnands, A. Patruno, D. Altamirano, J. Homan, S. Bogdanov, D. Pooley, arXiv:1310.7937 (2013)
219. A. Papitto, E. Bozzo, C. Ferrigno, L. Pavan, P. Romano, S. Campana, *ATel* **4959**, 1 (2013)
220. M. Linares, *ATel* **4960**, 1 (2013)
221. M. Serino, T. Takagi, et al., *ATel* **4961**, 1 (2013)
222. A. Patruno, *ATel* **5068**, 1 (2013)
223. C. Pallanca, E. Dalessandro, F.R. Ferraro, B. Lanzoni, G. Beccari, *ApJ* **773**, 122 (2013)
224. H.N. Cohn, P.M. Lugger, S. Bogdanov, C.O. Heinke, M. Van Den Berg, G. Sivakoff, *ATel* **5031**, 1 (2013)
225. A. Papitto, J.W.T. Hessels, M. Burgay, S. Ransom, N. Rea, A. Possenti, I. Stairs, C. Ferrigno, E. Bozz, *ATel* **5069**, 1 (2013)
226. P. Ghosh, F.K. Lamb, *ApJ* **223**, L83 (1978)
227. P. Ghosh, F.K. Lamb, *ApJ* **234**, 296 (1979)
228. P. Ghosh, F.K. Lamb, *ApJ* **232**, 259 (1979)
229. D. Psaltis, D. Chakraborty, *ApJ* **521**, 332 (1999)
230. N.I. Shakura, R.A. Syunyaev, *A&A* **24**, 337 (1973)
231. I.D. Novikov, K.S. Thorne, in *Black Holes (Les Astres Occlus)*, ed. by C. Dewitt, B.S. Dewitt (1973), pp. 343–450
232. Y.M. Wang, *A&A* **183**, 257 (1987)
233. S.A. Rappaport, J.M. Fregeau, H. Spruit, *ApJ* **606**, 436 (2004)
234. T.M. Tauris, *Science* **335**, 561 (2012)
235. D.R. Lorimer, M. Kramer, *Handbook of Pulsar Astronomy* (2004)

236. T. Tauris, N. Langer, M. Kramer, submitted to MNRAS (2012)
237. Spitkovsky, A. 2006, ApJ , 648, L51
238. N. Andersson, K. Glampedakis, B. Haskell, A.L. Watts, MNRAS **361**, 1153 (2005)
239. A. Patruno, B. Haskell, C. D'Angelo, ApJ **746**, 9 (2012)
240. C.O. Heinke, P.G. Jonker, R. Wijnands, C.J. Deloye, R.E. Taam, ApJ **691**, 1035 (2009)
241. A.F. Illarionov, R.A. Sunyaev, A&A **39**, 185 (1975)
242. M.M. Romanova, G.V. Ustyugova, A.V. Koldoba, R.V.E. Lovelace, ApJ **635**, L165 (2005)
243. G.V. Ustyugova, A.V. Koldoba, M.M. Romanova, R.V.E. Lovelace, ApJ **646**, 304 (2006)
244. A. Papitto, M.T. Menna, L. Burderi, T. Di Salvo, F. D'Antona, N.R. Robba, ApJ **621**, L113 (2005)
245. C. Lange, F. Camilo, N. Wex, M. Kramer, D.C. Backer, A.G. Lyne, O. Doroshenko, MNRAS **326**, 274 (2001)
246. L. Burderi, T. Di Salvo, M.T. Menna, A. Riggio, A. Papitto, ApJ **653**, L133 (2006)
247. A. Patruno, J.M. Hartman, R. Wijnands, D. Chakrabarty, M. van der Klis, ApJ **690**, 1856 (2009)
248. B. Haskell, A. Patruno, ApJ **738**, L14 (2011)
249. A. Patruno, R. Wijnands, M. van der Klis, ApJ **698**, L60 (2009)
250. M. van der Klis, ApJ **561**, 943 (2001)
251. A.L. Watts, A. Patruno, M. van der Klis, ApJ **688**, L37 (2008)
252. M. Bachetti, M.M. Romanova, A. Kulkarni, L. Burderi, T. di Salvo, MNRAS **403**, 1193 (2010)
253. F.K. Lamb, S. Boutloukos, S. Van Wassenhove, R.T. Chamberlain, K.H. Lo, A. Clare, W. Yu, M.C. Miller, ApJ **706**, 417 (2009)
254. M.M. Romanova, G.V. Ustyugova, A.V. Koldoba, R.V.E. Lovelace, ApJ **610**, 920 (2004)
255. M. Ruderman, ApJ **366**, 261 (1991)
256. M. Long, M.M. Romanova, F.K. Lamb, New Astronomy **17**, 232 (2012)
257. F.K. Lamb, D. Pines, J. Shaham, ApJ **225**, 582 (1978)
258. F.K. Lamb, J. Shaham, D. Pines, ApJ **224**, 969 (1978)
259. J.E. Deeter, P.E. Boynton, F.K. Lamb, G. Zylstra, ApJ **336**, 376 (1989)
260. J. Poutanen, M. Gierliński, MNRAS **343**, 1301 (2003)
261. J. Poutanen, in *A Decade of Accreting Millisecond X-Ray Pulsars, AIPC Series*, vol. 1068, pp. 77-86, ed. by R. Wijnands, et al. (2008)
262. D.A. Leahy, S.M. Morsink, Y.Y. Chung, Y. Chou, ApJ **691**, 1235 (2009)
263. D.A. Leahy, S.M. Morsink, Y. Chou, ApJ **742**, 17 (2011)
264. S.M. Morsink, D.A. Leahy, ApJ **726**, 56 (2011)
265. C. Cadeau, S.M. Morsink, D. Leahy, S.S. Campbell, ApJ **654**, 458 (2007)
266. M.P. Muno, F. Özel, D. Chakrabarty, ApJ **581**, 550 (2002)
267. J. Poutanen, *Advances in Space Research* **38**, 2697 (2006)
268. J. Poutanen, A.M. Beloborodov, MNRAS **373**, 836 (2006)
269. R.Z. Yahel, A&A **90**, 26 (1980)
270. T. Bulik, H. Riffert, P. Meszaros, K. Makishima, T. Mihara, B. Thomas, ApJ **444**, 405 (1995)
271. U. Kraus, S. Blum, J. Schulte, H. Ruder, P. Meszaros, ApJ **467**, 794 (1996)
272. M. Annala, J. Poutanen, A&A **520**, A76 (2010)
273. M. Long, M.M. Romanova, R.V.E. Lovelace, MNRAS **386**, 1274 (2008)
274. A.K. Kulkarni, M.M. Romanova, ApJ **633**, 349 (2005)
275. W. Cui, E.H. Morgan, L.G. Titarchuk, ApJ **504**, L27+ (1998)
276. A.L. Watts, T.E. Strohmayer, MNRAS **373**, 769 (2006)
277. J.M. Hartman, A.L. Watts, D. Chakrabarty, ApJ **697**, 2102 (2009)
278. J.J.E. Kajava, A. Ibragimov, M. Annala, A. Patruno, J. Poutanen, MNRAS **417**, 1454 (2011)
279. J. Poutanen, A. Ibragimov, M. Annala, ApJ **706**, L129 (2009)
280. B. Paczyński, *Acta Astron.* **17**, 287 (1967)
281. T. di Salvo, L. Burderi, A. Riggio, A. Papitto, M.T. Menna, MNRAS **389**, 1851 (2008)
282. L. Burderi, A. Riggio, T. di Salvo, A. Papitto, M.T. Menna, A. D'Ai, R. Iaria, A&A **496**, L17 (2009)
283. K. Lazaridis, J.P.W. Verbiest, et al., MNRAS **414**, 3134 (2011)

284. A. Riggio, L. Burderi, T. di Salvo, A. Papitto, A. D'Ai, R. Iaria, M.T. Menna, *A&A* **531**, A140 (2011)
285. J.M. Lattimer, M. Prakash, *Science* **304**, 536 (2004)
286. J.M. Lattimer, M. Prakash, *Phys. Rep.* **442**, 109 (2007)
287. D. Chakrabarty, in *A Decade of Accreting Millisecond X-Ray Pulsars*, *AIPC Series*, vol. 1068, pp. 67–74, ed. by R. Wijnands, et al. (2008)
288. A.L. Watts, *ARA&A* **50**, 609 (2012)
289. J.W.T. Hessels, S.M. Ransom, I.H. Stairs, P.C.C. Freire, V.M. Kaspi, F. Camilo, *Science* **311**, 1901 (2006)
290. R.W. Romani, *Nature* **347**, 741 (1990)
291. R.A.M.J. Wijers, *MNRAS* **287**, 607 (1997)
292. R.A.M.J. Wijers, in *Pulsar Timing, General Relativity and the Internal Structure of Neutron Stars*, ed. by Z. Arzoumanian, F. Van der Hooft, & E. P. J. van den Heuvel (1999), p. 293
293. A.R. Choudhuri, S. Konar, *MNRAS* **332**, 933 (2002)
294. S. Konar, A.R. Choudhuri, *MNRAS* **348**, 661 (2004)
295. M. Bejger, M. Fortin, P. Haensel, J.L. Zdunik, *A&A* **536**, A87 (2011)
296. G.S. Bisnovatyi-Kogan, B.V. Komberg, *Soviet Ast.* **18**, 217 (1974)
297. A. Cumming, E. Zweibel, L. Bildsten, *ApJ* **557**, 958 (2001)
298. J. Brainerd, F.K. Lamb, *ApJ* **317**, L33 (1987)
299. L. Titarchuk, W. Cui, K. Wood, *ApJ* (2002)
300. L. Titarchuk, S. Kuznetsov, N. Shaposhnikov, *ApJ* **667**, 404 (2007)
301. F. Özel, *ApJ* **691**, 1678 (2009)
302. K.S. Wood, C. Ftaclas, M. Kearney, *ApJ* **324**, L63 (1988)
303. M.M. Romanova, A.K. Kulkarni, R.V.E. Lovelace, *ApJ* **673**, L171 (2008)
304. C.G. Bernal, D. Page, W.H. Lee, *ApJ* **770**, 106 (2013)
305. D. Mukherjee, D. Bhattacharya, A. Mignone, *MNRAS* **435**, 718 (2013)
306. D.J.B. Payne, A. Melatos, *MNRAS* **376**, 609 (2007)
307. D.J.B. Payne, A. Melatos, *MNRAS* **351**, 569 (2004)
308. E. Göğüş, M.A. Alpar, M. Gilfanov, *ApJ* **659**, 580 (2007)
309. A.M. Beloborodov, *ApJ* **566**, L85 (2002)
310. K. Viironen, J. Poutanen, *A&A* **426**, 985 (2004)
311. F.K. Lamb, S. Boutloukos, S. Van Wassenhove, R.T. Chamberlain, K.H. Lo, M.C. Miller, *ApJ* **705**, L36 (2009)
312. J. Arons, S.M. Lea, *ApJ* **207**, 914 (1976)
313. R.F. Elsner, F.K. Lamb, *ApJ* **215**, 897 (1977)
314. A.K. Kulkarni, M.M. Romanova, *MNRAS* **386**, 673 (2008)
315. S. Bhattacharyya, T.E. Strohmayer, *ApJ* **641**, L53 (2006)
316. S. Bhattacharyya, T.E. Strohmayer, *ApJ* **656**, 414 (2007)
317. D.K. Galloway, M.P. Muno, J.M. Hartman, D. Psaltis, D. Chakrabarty, *ApJS* **179**, 360 (2008)
318. T.E. Strohmayer, C.B. Markwardt, J.H. Swank, J. in't Zand, *ApJ* **596**, L67 (2003)
319. S. Bhattacharyya, T.E. Strohmayer, M.C. Miller, C.B. Markwardt, *ApJ* **619**, 483 (2005)
320. A.L. Watts, T.E. Strohmayer, C.B. Markwardt, *ApJ* **634**, 547 (2005)
321. A.L. Watts, T.E. Strohmayer, *MNRAS* **373**, 769 (2006)
322. K. Koyama, H. Inoue, et al., *ApJ* **247**, L27 (1981)
323. M. Czerny, B. Czerny, J.E. Grindlay, *ApJ* **312**, 122 (1987)
324. W.H.G. Lewin, J. van Paradijs, R.E. Taam, *Space Science Reviews* **62**, 223 (1993)
325. M.P. Muno, D. Chakrabarty, D.K. Galloway, P. Savov, *ApJ* **553**, L157 (2001)
326. M.P. Muno, D.K. Galloway, D. Chakrabarty, *ApJ* **608**, 930 (2004)
327. P. Kaaret, J.J.M. i. Zand, J. Heise, J.A. Tomsick, *ApJ* **598**, 481 (2003)
328. P. Kaaret, E.H. Morgan, R. Vanderspek, J.A. Tomsick, *ApJ* **638**, 963 (2006)
329. A.L. Watts, D. Altamirano, M. Linares, A. Patruno, P. Casella, Y. Cavecchi, N. Degenaar, N. Rea, P. Soleri, M. van der Klis, R. Wijnands, *ApJ* **698**, L174 (2009)
330. M. Falanga, L. Kuiper, J. Poutanen, D.K. Galloway, E.W. Bonning, E. Bozzo, A. Goldwurm, W. Hermsen, L. Stella, *A&A* **529**, A68 (2011)
331. A. Riggio, L. Burderi, et al., *ATel* **5086**, 1 (2013)

332. S. Motta, A. D’Ai, A. Papitto, A. Riggio, T. di Salvo, L. Burderi, T. Belloni, L. Stella, R. Iaria, *MNRAS* **414**, 1508 (2011)
333. M. Chakraborty, S. Bhattacharyya, *ApJ* **730**, L23 (2011)
334. M. Chakraborty, S. Bhattacharyya, A. Mukherjee, *MNRAS* **418**, 490 (2011)
335. M. Linares, D. Chakraborty, M. van der Klis, *ApJ* **733**, L17 (2011)
336. M. Linares, D. Altamirano, D. Chakraborty, A. Cumming, L. Keek, *ApJ* **748**, 82 (2012)
337. T. Strohmayer, L. Bildsten, *New views of thermonuclear bursts* (Compact stellar X-ray sources, 2006), pp. 113–156
338. M.Y. Fujimoto, T. Hanawa, S. Miyaji, *ApJ* **247**, 267 (1981)
339. R. Cornelisse, J.J.M. in’t Zand, F. Verbunt, E. Kuulkers, J. Heise, P.R. den Hartog, M. Cocchi, L. Natalucci, A. Bazzano, P. Ubertini, *A&A* **405**, 1033 (2003)
340. R. Narayan, J.S. Heyl, *ApJ* **599**, 419 (2003)
341. J.J.M. in’t Zand, P.G. Jonker, C.B. Markwardt, *A&A* **465**, 953 (2007)
342. E. Kuulkers, *Nuclear Physics B Proceedings Supplements* **132**, 466 (2004)
343. L. Keek, D.K. Galloway, J.J.M. in’t Zand, A. Heger, *ApJ* **718**, 292 (2010)
344. J.M. Hartman, D. Chakraborty, D.K. Galloway, M.P. Muno, P. Savov, M. Mendez, S. van Straaten, T. Di Salvo, *BAAS* **35**, 865 (2003)
345. A. Spitkovsky, Y. Levin, G. Ushomirsky, *ApJ* **566**, 1018 (2002)
346. A. Heger, A. Cumming, S.E. Woosley, *ApJ* **665**, 1311 (2007)
347. M. Revnivtsev, E. Churazov, M. Gilfanov, R. Sunyaev, *A&A* **372**, 138 (2001)
348. T.E. Strohmayer, W. Zhang, J.H. Swank, A. Smale, L. Titarchuk, C. Day, U. Lee, *ApJ* **469**, L9+ (1996)
349. T.E. Strohmayer, W. Zhang, J.H. Swank, I. Lapidus, *ApJ* **503**, L147 (1998)
350. M.P. Muno, D. Chakraborty, D.K. Galloway, D. Psaltis, *ApJ* **580**, 1048 (2002)
351. M.P. Muno, F. Özel, D. Chakraborty, *ApJ* **595**, 1066 (2003)
352. M. Gierliński, C. Done, *MNRAS* **337**, 1373 (2002)
353. M.G.F. Kirsch, K. Mukerjee, M.G. Breielfellner, S. Djavidnia, M.J. Freyberg, E. Kendziorra, M.J.S. Smith, *A&A* **423**, L9 (2004)
354. M. Gierliński, J. Poutanen, *MNRAS* **359**, 1261 (2005)
355. M.M. Shara, *ApJ* **261**, 649 (1982)
356. E.F. Brown, L. Bildsten, *ApJ* **496**, 915 (1998)
357. J.S. Heyl, *ApJ* **600**, 939 (2004)
358. A.L. Piro, L. Bildsten, *ApJ* **629**, 438 (2005)
359. K. Heng, A. Spitkovsky, *ApJ* **703**, 1819 (2009)
360. M.C. Miller, F.K. Lamb, D. Psaltis, *ApJ* **508**, 791 (1998)
361. M. Méndez, T. Belloni, *MNRAS* **381**, 790 (2007)
362. H.X. Yin, C.M. Zhang, Y.H. Zhao, Y.J. Lei, J.L. Qu, L.M. Song, F. Zhang, *A&A* **471**, 381 (2007)
363. F.K. Lamb, M.C. Miller, arXiv:0308179 (2003)
364. W. Kluźniak, M.A. Abramowicz, *Ap&SS* **300**, 143 (2005)
365. L. Stella, M. Vietri, *Physical Review Letters* **82**, 17 (1999)
366. L. Stella, M. Vietri, *ApJ* **492**, L59+ (1998)
367. J. Dexter, P.C. Fragile, *ApJ* **730**, 36 (2011)
368. A. Ingram, C. Done, *MNRAS* **415**, 2323 (2011)
369. A. Ingram, C. Done, *MNRAS* **419**, 2369 (2012)